A Simulation of Biological Processes in the Equatorial Pacific Warm Pool at 165°E

by

Charles R. McClain
SeaWiFS Project Office
Laboratory for Hydrospheric Processes
NASA Goddard Space Flight Center
Greenbelt, Maryland

Ragu Murtugudde
Joint Center for Earth System Sciences
University of Maryland
College Park, Maryland

and

Sergio Signorini
SAIC*/General Sciences Corporation
Laurel, Maryland

*Science Applications International Corporation

Abstract

A nine-year simulation (1984-1992) of biological processes in the equatorial Pacific

Warm Pool is presented. A modified version of the 4-component (phytoplankton, zooplankton,

nitrate and ammonium) ecosystem model by McClain et al. (1996) is used. Modifications

include use of a spectral model for computation of PAR and inclusion of fecal pellet

remineralization and ammonium nitrification. The physical parameters (horizontal and vertical

velocities and temperature) required by the ecosystem model were derived from an improved

version of the Gent and Cane (1990) ocean general circulation model (Murtugudde and

Busalacchi, 1997). Surface downwelling spectral irradiance was estimated using the clear-sky

models of Frouin et al. (1989) and Gregg and Carder (1990) and cloud cover information from

the International Satellite Cloud Climatology Project (ISCCP).

The simulations indicate considerable variability on interannual time scales in all four

ecosystem components. In particular, surface chlorophyll concentrations varied by an order of

magnitude with maximum values exceeding 0.30 mg·m^{-3} in 1988, 1989, and 1990, and

pronounced minimums during 1987 and 1992. The deep chlorophyll maximum ranged between

75 and 125 meters with values occasionally exceeding 0.40 mg·m^{-3}. With the exception of the

last half of 1988, surface nitrate was always near depletion. Ammonium exhibited a subsurface

maximum just below the DCM with concentrations as high as 0.5 mg-atN·m^{-3}. Total integrated

annual primary production varied between 40 and 250 gC·m^{-2}·yr^{-1} with an annual average of 140

gC·m^{-2}·yr^{-1}.

Finally, the model is used to estimate the mean irradiance at the base of the mixed layer,

i.e., the penetration irradiance, which was 18 Watts·m^{-2} over the nine year period. The average

mixed layer depth was 42 m.

Introduction

The equatorial Pacific is generally discussed in term of two regimes denoted as the "Cold Tongue" in the east and the "Warm Pool" in the west. Biologically, the Cold Tongue is considered to be one of the most productive ecosystems in the world (Chavez and Barber, 1987) and was the site of one of the Joint Global Ocean Flux Study (JGOFS) process experiments (Murray, et al., 1995). On the other hand, the biological processes in the Warm Pool have received relatively little attention, but is of particular interest to the physical oceanography and meteorology communities because of its role in heat and moisture fluxes between the ocean and the atmosphere and, consequently, El Niño and the Southern Oscillation. For example, the Tropical Ocean Global Atmosphere (TOGA) program (Delcroix and Henin, 1991; McPhaden and Hayes, 1991) conducted a special experiment, the Coupled Ocean Atmosphere Response Experiment (COARE) in the Warm Pool during November 1992 though February 1993 (Webster and Lukas, 1992).

The Warm Pool is characterized by some of the warmest SSTs in the global ocean and has a shallow mixed layer (30-40 m) separated from the thermocline (deeper than 65 m) by a high salinity barrier layer (Lukas and Lindstrom, 1991). Data from the Warm Pool have been analyzed extensively to study the physical dynamics (Delcroix and Henin, 1988), SST variability (McPhaden and Hayes, 1991), surface layer variations (Sprintall and McPhaden, 1994), heat balance (Cronin and McPhaden, 1997), and other ENSO related processes (Delcroix et al., 1992; Delcroix et al., 1993; Picaut et al., 1996). Generally, heat budget and circulation studies focus on the surface fluxes, but, as noted by Lewis et al. (1990) and Siegel et al. (1995), variations in the amount of irradiance penetrating though the mixed layer are largely due to changes in

phytoplankton abundance, especially in the Warm Pool where the mixed layer depth (MLD) is relatively constant, and can significantly influence the heat budget. Relatively small changes in sea surface temperature and mixed layer heat content in the Warm Pool can stimulate a substantial response in large scale weather patterns (Palmer and Mansfield, 1984). Thus, there are very good reasons for understanding the biological processes in the Warm Pool that are quite different from the primary objectives of programs such as JGOFS.

Some measurements of biological properties in the Warm Pool are available (Furuya, 1990; Barber and Chavez, 1991; Blanchot et al., 1992; Machey et al., 1995 and 1997; Radenac and Rodier, 1996; Dupouy et al., 1997). While the cumulative data set is inadequate for characterizing the horizontal and temporal variability, the data do show large variations in the vertical distribution of phytoplankton within the Warm Pool. Barber and Chavez (1991) describe zonal variability across the basin and show (1) the deep chlorophyll maximum (DCM) deepens from about 50 meters east of the dateline to 100 meters west of the dateline, (2) iron is not limiting in the western equatorial Pacific, and (3) annual production in the Warm Pool is 90-120 $gC \cdot m^{-2} \cdot yr^{-1}$. Their annual production values are 2-3 times higher than most historical climatologies indicate (Berger, 1989). Climatological nitrate (NO_3^-) concentrations are less the 1 $mg\text{-}atN \cdot m^{-3}$ in the top 40 meters (Conkright et al., 1994) which corresponds to the mixed layer. Mackey et al. (1995) and Radenac and Rodier (1996) both discuss the relative depths of the nitracline, the mixed layer, and the influence of low salinity water on the distribution of chlorophyll and nutrients. Both groups emphasize the suppression of nutrient fluxes by the high salinity barrier layer as the primary factor controlling surface phytoplankton concentrations in the Warm Pool. Finally, Leonard and McClain (1996) partitioned the Warm Pool into northern and

southern sectors using the CZCS data set and demonstrated that surface pigment concentrations, on interannual time scales, were strongly correlated with sea level and, presumably, thermocline variations associated with the 1982-1983 El Niño, but found no correlation with SST. The CZCS pigment concentrations which normally ranged between 0.05-0.10 $mg \cdot m^{-3}$ in the Warm Pool increased by at least a factor of two during the event.

The objectives of this study are to use a simple ecosystem model to examine, in more detail than observations allow, (1) the temporal variability of the ecosystem in response to physical forcing, (2) the relative influences of mixing and upwelling on the biological variability, and (3) the vertical distribution of biological properties and processes . The ecosystem model has been previously coupled to the Garwood (1977; see McClain et al., 1996) and the Chen et al. (1994; see McClain et al. 1998) mixed layer models. However, for this study, the ecosystem model is not coupled to the physical model because a simple one-dimensional mixed layer model cannot adequately simulate the physical processes in this region where remotely forced vertical modulations of the thermocline are substantial. These vertical excursions of the thermocline and, therefore, the nitracline, have a profound influence on the availability of nutrients to the euphotic zone. Therefore, the physical oceanic inputs (u, v, w, T) were provided from a basin-scale simulation using the Murtugudde and Busalacchi (1997) ocean general circulation model (OGCM) which has the Chen et al. (1994) mixed layer model embedded in it. Thus, there is no feedback to the physical model from the ecosystem model, e.g. time-dependent diffuse attenuation. The next phase of the model development will be to link the physical and ecosystem models over the entire physical model domain in order to examine the biological feedbacks on the physical system.

The use of a one-dimensional ecosystem model at 165°E can be justified because this location is not significantly affected by horizontal advection. The heat budget analyses of the TOGA-COARE domain by Gent (1991) with an OGCM has already shown that the advective effects in the region are small because of weak currents and very weak temperature gradients. Also, similarly weak gradients in nutrients support this assumption. Figure 1 shows the nitrate concentration climatology of Conkright et al. (1994) and its zonal derivative. The 165°E site is near the region of lowest concentrations and zonal variation above 250 m. Picaut et al. (1996) proposed that the eastern edge of the warm pool migrates zonally in the equatorial wave guide over several degrees of longitude. Our OGCM does reproduce the zonal migration of the warm pool accurately (Picaut et al., 1996) and shows that during the period of this study here, the warm pool moved to the west of 165°E during the La Niñas of 1984 and 1988-1989. The upwelling and the flow fields used to compute the vertical mixing account for these effects and the ecosystem model behaves as expected with no apparent anomalous effects during these periods.

Model Description

The simulation incorporates outputs from the basin scale circulation model, an atmospheric radiative transfer model and the ecosystem model (includes the marine optical model). The circulation model is fully described in Murtugudde and Busalacchi (1997) and will not be discussed in detail here. The atmospheric radiative transfer model extends the approach described in McClain et al. (1996) to accommodate spectral irradiance and a different scheme for the cloud cover correction. The ecosystem model is a modified version of the model developed by McClain et al. (1996). The atmospheric radiative transfer model and the modifications to the

McClain et al. (1996) ecosystem model are outlined below.

Atmospheric Radiative Transfer Model

As will be described in the following section, the ecosystem model requires spectral

irradiance, so the model of Gregg and Carder (1990) was used to compute the clear sky

irradiance at ultraviolet and visible wavelengths from 280-700 nm. The published version of

their model only includes 350-700 nm (PAR, Photosynthetically Active Radiation), but is easily

extended to include shorter wavelengths given the solar constants and ozone absorption

coefficients for those wavelengths. Gregg and Carder's algorithm requires estimates of surface

wind speed, humidity, precipitable water, visibility and ozone concentrations. Table 1 provides

information on these ancillary data.

While the computation of clear sky irradiance is straightforward, accounting for light

attenuation by clouds is not. Total surface irradiance observations are available from a few

moorings of the TAO array, but are not available for the location and time period of interest in

this study. Total monthly mean surface irradiance and cloud fraction estimates from the

International Satellite Cloud Cover Project (ISCCP; Schiffer and Rossow, 1985) are only

available for July 1983 through December 1992. ISCCP surface PAR estimates (Bishop and

Rossow, 1991; Bishop et al., 1997) were not available for the time period of interest when this

study was initiated. Therefore, an algorithm for calculating the visible surface spectral irradiance

using theoretical clear sky irradiance models and estimates of monthly mean total irradiances and

cloud cover from the ISCCP data set was developed and, presumably, would be valid for any

other time period at this location.

The approach emulates the ISCCP processing by using a formulation which incorporates coefficients derived from statistical comparisons with ISCCP data. ISCCP total (tot) surface irradiance (250-4000 nm) and PAR are approximated using

$$E_I^{'}(tot) = E_F^c(tot) \cdot C_I^{'} \tag{1}$$

$$E_I^{'}(PAR) = E_F^c(PAR) \cdot C_I^{'} \tag{2}$$

where $E_I^{'}(tot)$ and $E_I^{'}(PAR)$ are the equivalent ISCCP irradiances. $E_F^c(tot)$ and $E_F^c(PAR)$ are clear sky irradiances computed using Frouin et al. (1989). $C_I^{'}$ is the equivalent ISCCP cloud cover correction. The Frouin et al. algorithm requires water vapor (precipitable water), visibility and ozone inputs. A marine haze model is assumed. The cloud cover correction is assumed to be independent of wavelength, at least to the first order. On average, $E_F^c(PAR) \approx E_F^c(tot)/2$.

To estimate $C_I^{'}$ using ISCCP cloud fraction data, the cloud correction scheme of Dobson and Smith (1988) is adopted, i.e.,

$$E_{DS}(tot) = E_o(tot) \cdot \cos\theta_o (A_i + B_i \cos\theta_o) \tag{3}$$

where E_{DS} is the Dobson and Smith estimate of total irradiance, E_o is the extraterrestrial irradiance, θ_o is the solar zenith angle, and A_i and B_i are empirical constants where (i) is the cloud okta index (0-8) with 0 designating clear conditions and 8 being totally overcast.

Dividing (3) by (1) yields

$$\frac{E_{DS}(tot)}{E_I^{'}(tot)} = \left(\frac{E_{DS}^c(tot)}{E_F^c(tot)}\right) \cdot \left(\frac{C_{DS}}{C_I^{'}}\right) \tag{4}$$

where

$$E_{DS}^c(tot) = E_o(tot) \cdot \cos\theta_o (A_c + B_c \cos\theta_o) \tag{5}$$

and

$$C_{DS} = \frac{A_i + B_i \cos\theta_o}{A_c + B_c \cos\theta_o} \tag{6}$$

Comparison of monthly mean values of $E_{DS}(tot)$ computed using monthly mean cloud cover with the actual $E_I(tot)$ values from the ISCCP data set yielded a mean ratio of 1.11 for the left side of equation (4). Similarly, an annual cycle of E_F^c compared with E_{DS}^c values produced an fairly constant ratio of 0.95 for the first ratio on the right side of (4). It is assumed that these ratios are independent of wavelength and can be applied in the visible. Thus,

$$E_I^{'}(tot) \approx 0.85 \cdot E_F^c(tot) \cdot C_{DS} \tag{7}$$

Frouin et al. provide algorithms for both PAR and total surface irradiance while Gregg and Carder (1990) only address spectral PAR. Because spectral PAR is required, equation 2 can be generalized for each wavelength, and, by making the appropriate substitutions, the following expression is derived.

$$E_I'(\lambda) \approx 0.85 \cdot R_{PAR} \cdot E_{GC}^c(\lambda) \cdot C_{DS} \qquad (8)$$

where $R_{PAR} = E_F^c(PAR)/E_{GC}^c(PAR)$ at each time step. On average, R_{PAR} is 1.01. No smoothing of

the monthly mean cloud fraction was included in the model surface irradiance computation.

Figure 2 provides the time series of $E_F^c(PAR)$, monthly mean cloud cover fraction, and

$E_I'(PAR)$. The interannual changes in cloud cover are particularly evident in the 1987 and 1988

data, corresponding to a transition from warm to cool SSTs. A comparison results from this

method with those of Bishop et al. (1997) for 1987 through 1990 indicate that (1) the daily

average clear sky total irradiances (≈ 300 W·m^{-2}) agree to within 3%, and (2) the daily average

cloud-corrected total irradiances (≈ 242 W·m^{-2}) agree to within 1%.

Ecosystem Model

The ecosystem model (Figure 3) is essentially the same as that used in McClain et al.

(1996), although a number of modifications have been made as described below. Figure 3 also

includes the nitrogen fluxes which will be discussed later.

The most significant change in the ecosystem model from that used in McClain et al.

(1996) is the incorporation of the spectral light model with spectral absorption from 280 to 700

nm. The spectral light model requires absorption spectra for water and chlorophyll-a. The

absorption spectra of Baker and Smith (1982) and Dupouy et al. (1997) for seawater and

phytoplankton, respectively, were used (Figure 4). Use of a spectral model eliminated the need

to estimate light attenuation for PAR, i.e. K(PAR), using the Morel (1988) empirical function

based on chlorophyll-a concentration. Also, the growth rate and C:Chl-a (carbon to chlorophyll-

a) ratio computations require integrations over PAR in units of μE (microEinsteins). The transformation from Watts·m^{-2}·nm^{-1} to μE·m^{-2}·s^{-1}·nm^{-1} was applied to each wavelength according to the expression (Zeebe et al., 1996),

$$E^{\mu E}(\lambda) = \frac{E^{W}\lambda \cdot 10^{6}}{N_{A}hc} \qquad (9)$$

where N_A is Avogadro's number (6.022·10^{23} mol^{-1}), h is Planck's constant (6.626·10^{-34} J·s), c is the speed of light (2.998·10^8 m·s^{-1}), and λ is in meters.

The surface wind stress dependent algorithm for the eddy diffusion, K_v, has been replaced with the method of Pacanowski and Philander (1981) which utilizes profiles of temperature and horizontal currents (u and v) which, in the present case, are obtained independently from the ocean circulation model (described below). A background value of 8 m^{2}d^{-1} is assumed. Similarly, the vertical velocity, w, is also obtained from the ocean circulation model rather than being derived from the curl of the local wind stress because of the singularity in the Ekman formulation for w at the equator and because remote forcing of local fields must be accounted for at this site (Kessler, 1990).

The bottom boundary (250 m) nitrate concentration is allowed to change as a function of temperature, T (°C). A variable bottom boundary condition was needed because planetary waves introduce significant vertical excursions of the isopycnal surfaces below 250 m. Using climatological nutrient data at 165°E from Conkright et al. (1994) for the five standard depths between 150 and 400 m,

$$NO_3(250) = 39.64 - 1.467 \cdot T(250) \tag{10}$$

with an $r^2 = 0.92$.

The exponential temperature-dependent zooplankton respiration rate (r_z) algorithm has been replaced with a linear relationship based on data from Ikeda (1985) for the tropics. The linear respiration relationship,

$$r_z = 0.0722 + 0.0067(T - 20), \tag{11}$$

produces rates less than 0.15 d^{-1}.

Several changes in the phytoplankton terms were made. The half saturation constant for NH_4^+, K_{NH4}, was increased from to 0.1 to 0.5. Also, the NH_4^+ inhibition coefficient, pk, was increased from 3 to 5. These changes were introduced to help limit phytoplankton growth rates to a range consistent with observed values since maximum growth rates (Eppley, 1972) are potentially as high as 3.5 at the surface temperatures (28°C to 30°C) in the Warm Pool. Also, the value of G_0 in the phytoplankton growth rate equation derived from Eppley (1972) was reduced to 0.591 as a result of a reinterpretation of the Eppley results (J. Christian, personal communication). Phytoplankton mortality, m, was increased from 0 to 0.1 in recognition that losses other than zooplankton grazing do occur. Phytoplankton sinking was set to 0 to reflect the fact that cell sizes are relatively small in the Warm Pool (Blanchot et al., 1992) and do not sink at an appreciable rate. Finally, the C:Chl-a relationship of Cloern et al. (1995) is used. The observed range appears to be about 20 to 300 µgC/µgChl-a (Furuya, 1990; Chavez et al., 1996)

for the equatorial Pacific.

Fecal pellet remineralization, to NH_4^+, has been added as a constant fraction (c_{pel}) of the fecal pellet production. The model used at OWS P did not include this process. About 70% of the pellets are recycled in the photic layer of the HNLC (high nutrient-low chlorophyll; Dam et al., 1995) eastern equatorial Pacific and 84% (Le Borgne and Rodier, 1997) in the oligotrophic regions of the equatorial Pacific. A value of $c_{pel} = 0.8$ was used.

In McClain et al. (1996), the vertical distribution of ammonium at depth was controlled by the fixed bottom boundary value and resulted in an unrealistically broad subsurface maximum below the euphotic zone. This condition was remedied (McClain et al., 1998) by incorporating an ammonium nitrification algorithm based on Olson (1981). The algorithm requires a spectral light model for computation of the irradiation dosage between 300-470 nm to incur inhibition of bacterial conversion of NH_4^+ to NO_3^- near the surface. The addition of this process enables the model to reproduce the observed subsurface NH_4^+ maxima between 60-120 m (J. Murray, personal communication). The rate of conversion of ammonium to nitrate, A^n, is

$$A^n = A^n_{max}\left(1 - \frac{D - D_{min}}{D - D_{min} + K_D}\right), \tag{12}$$

where

$$D = \int_0^{24} \int_{300}^{470} E_s(\lambda, t)\alpha(\lambda)d\lambda dt \tag{13}$$

$D_{min} = 0.0095$ $W{\cdot}m^{-2}$, $A^n_{max} = 0.002$ mg-atN${\cdot}$m^{-3}d^{-1}, $K_D = 0.036$ $W{\cdot}m^{-2}$, and E_s has units of

$W{\cdot}m^{-2}{\cdot}nm^{-1}$. K_D is the half-saturation dosage or the dosage at which inhibition is half the maximum rate, and D_{min} is the minimum inhibition dosage. $\alpha(\lambda)$ is the action spectrum for photoinhibition of *Nitrosomonas europaea* taken from Olson (1981).

Thus, the final set of model equations are

$$\frac{\partial P}{\partial t} + w_e \frac{\partial P}{\partial z} + \frac{\partial SP}{\partial z} - \frac{\partial}{\partial z}\left(K_v \frac{\partial P}{\partial z}\right) = GP - mP - r_p P - IZ \tag{14}$$

$$\frac{\partial Z}{\partial t} + w_e \frac{\partial Z}{\partial z} - \frac{\partial}{\partial z}\left(K_v \frac{\partial Z}{\partial z}\right) = (1-\gamma)IZ - gZ - r_z Z \tag{15}$$

$$\frac{\partial NH_4^+}{\partial t} + w\frac{\partial NH_4^+}{\partial z} - \frac{\partial}{\partial z}\left(K_v \frac{\partial NH_4^+}{\partial z}\right) = \left(a_p m + r_p - \pi_1 G\right)P + \left(a_z g + r_z + c_{pel}\gamma I\right)Z - A^n \tag{16}$$

$$\frac{\partial NO_3^-}{\partial t} + w\frac{\partial NO_3^-}{\partial z} - \frac{\partial}{\partial z}\left(K_v \frac{\partial NO_3^-}{\partial z}\right) = -\pi_2 GP + A^n \tag{17}$$

Table 2 provides the variable definitions and the values of the free parameters used in deriving various terms in these equations. For the precise definitions of parameters not explicitly given, the reader is referred to McClain et al. (1996).

The Ocean Circulation Model

The OGCM is the reduced gravity, primitive equation, sigma coordinate model of Gent and Cane (1990) with an embedded hybrid mixing scheme (Chen et al., 1994). Surface heat fluxes are computed by coupling the OGCM to an advective atmospheric mixed layer model (Seager et al., 1995). Complete hydrology has been added to the model with freshwater forcing treated as a natural boundary condition (Huang, 1993). The UNESCO equation of state is used for computing buoyancy from salinity and temperature. The improvements in tropical SST simulations and upper ocean hydrology was reported in Murtugudde et al. (1996) and Murtugudde and Busalacchi (1997) respectively. The vertical structure of the model ocean consists of a mixed layer and a specified number of layers below according to a sigma coordinate (total number of layers is 30 for this simulation). The horizontal grid is stretched down to $\frac{1}{3}°$ resolution near the equator and at the eastern and western boundaries. The model domain spans the Pacific zonally with meridional boundaries at $\pm30°$ latitude. The MLD and the thickness of the deepest sigma layer are computed prognostically and the remaining layers are computed diagnostically such that the ratio of each sigma layer to the total depth below the mixed layer is held to its prescribed value. The model is spun up with climatological winds for 10 years. The interannual simulation for 1983-1992 is initialized with the climatological run and forced with the monthly mean FSU winds. The precipitation data of Xie and Arkin (1996) were used for freshwater forcing.

Results and Discussion

Circulation Model Fields

Figure 5 provides the depth-time plots of the physical parameters required by the ecosystem model, i.e., $E'_I(PAR)$, the OGCM vertical velocity, K_v (values derived from OGCM u, v, and T profiles), and temperature predictions at 165°E. The temperatures replicate the observed temperatures within the upper 100 m to within ±1°C, but are generally warmer at depth by 1-2°C, on average. Nonetheless, the OGCM does reproduce the temporal variations in the temperature such as the surface coolings during 1984 and 1988-1989 and the 60 m deepening of the 24°C isotherm between 1987 and 1989. The SSTs remain above 29°C and show little variability except during 1988-1989 La Niña when the 28°C isotherm reached the surface as in observations (McPhaden and Hayes, 1991). The depth of the thermocline (20°C isotherm) averages around 170 m. A slight deepening occurred during the1984 aftermath of the 1982-1983 El Niño. Another deepening occurred after the 1986-1987 El Niño and lasted until early 1990.

The dominant feature in the vertical structure of zonal currents at 165°E is the Equatorial Under Current (EUC). The core of the EUC typically lies above the thermocline except during the spring of 1985 and 1991 when the core was much deeper. The reversal of surface currents in the mixed layer merges with the eastward currents in the EUC which is also seen in observations (Figure 14 of McPhaden and Hayes, 1991; Figure 2 of Sprintall and McPhaden, 1994). The model EUC is slightly stronger and the core is shallower than observed and the reversals at the surface are more pronounced. These eastward surface currents in the model warm pool region are mainly caused by the model's manifestation of the Mindanao eddy extending too far equatorward due to closing of the Indonesian throughflow (see Murtugudde et al., 1998).

Delcroix and Henin (1988) noted the westward current below the EUC, the Equatorial

Intermediate Current (EIC). The EIC moves vertically with the EUC and is visible above 300m

depth sporadically (Sprintall and McPhaden, 1994). The weaker than observed model

thermocline is also seen as an EUC that is vertically more spread out than in observations.

The meridional currents are typically much smaller than zonal currents. The high

frequency of north-south reversals was noted by McPhaden and Hayes (1991) in daily averages.

Even the monthly mean forcing used in our model seems to retain some of this characteristic

albeit weaker in the magnitude of currents. The region just west of the dateline is dominated by

high frequency wind and freshwater forcing which are averaged out in our monthly mean forcing

of the model. As stated earlier, model results are also affected by the southward extension of the

Mindanao eddy.

The model current and temperature profiles are used within the ecosystem model to

estimate K_v (Figures 5 and 6a) at each depth and time step. The MLD (Figure 17) fluctuates

between 15 and 80 m and with a mean value of 42 m corresponding to about the 190 $m^2 \cdot d^{-1}$

isopleth. As expected, advances and retreats in the MLD generally correspond to high and low

K_v values, respectively, even though K_v is not explicitly provided by the OGCM, but is derived

from the OGCM u, v, and T fields using Pacanowski and Philander (1981).

The nature of the highly variable convergence and divergence at this location can be

easily inferred from the zonal and meridional currents described above. But as can be expected

by the one-dimensional nature of the heat balance in the region (see Cronin and McPhaden, 1997

and McPhaden and Hayes, 1991), the upwelling (Figures 5 and 6b) is mainly restricted to the

surface layer above the thermocline. Also, since the vertical temperature gradients are small, the

effects of upwelling on SST are small. The flow convergence (downwelling) is maximum in

October/November during the transition from the summer monsoon to the winter monsoon

resulting in maximum SSTs during this time. The signature of this wind-driven variability is

evident in the MLD variations. In a bulk mixed layer model, this region would have a shallow

MLD over much of the year due to low friction velocities (see Murtugudde et al., 1995). By

taking into account the mixing due to horizontal velocity shear and the convective adjustment

(see Chen et al., 1994), the model captures the high frequency mixed layer deepening. A large

westerly wind burst is seen in late 1990 which produces the largest MLD anomaly at 165° E.

Note that a prolonged El Niño occurred from 1991 through 1993.

Ecosystem Components and Derived Parameters: Comparisons with Observations

The ecosystem model computes profiles of the four ecosystem components at 1-hour

temporal and 1-m vertical resolutions. Figure 7 provides the depth-time contour plots of NH_4^+,

NO_3^-, chlorophyll (P), and Z. Barber and Chavez (1991) report that west of the dateline, surface

chlorophyll concentrations are less than 0.25 $mg \cdot m^{-3}$ and the DCM is between 75-125 m with a

value of about 0.4 $mg \cdot m^{-3}$. Model chlorophyll in the mixed layer varies from 0.01 to more than

0.30 on interannual time scales. Several of the annual mean vertical distributions (Figure 8) are

punctuated by a DCM between 80 and 120 meters. The climatological DCM is at 85 m with an

amplitude of 0.16 $mg \cdot m^{-3}$ (Figure 9). Figure 8 also indicates that the DCM is not always present,

even over extended periods as in 1988 and 1989. During 1987, and 1992, the surface values

were particularly low. Barber and Chavez (1991) estimate mean 0-60 m chlorophyll to be around

6 $mg \cdot m^{-2}$. The model produced a value of 7.2 $mg \cdot m^{-2}$ (the climatological profile has nearly

constant values ≈ 0.12 mg·m^{-3} from 0-60 m).

Blanchot et al. (1992) made meridional transects along 165°E during September 1987 and 1988 which highlight the interannual variability at this location. In September 1987, surface values were well below 0.1 mg·m^{-3} and the DCM exceeded 0.4 mg·m^{-3} at 80 m. Furuya (1990) present a very similar profile (DCM at 100 m) for October 1979 for the same location (Station 18). For September 1987, the model produced comparable values with very low values at the surface and a subsurface maximum of 0.42 mg·m^{-3} at around 120 m (monthly mean). In September 1988, the observed profile was much more uniform with concentrations of 0.3-0.4 mg·m^{-3} down to 100 m. The model concentrations are about 0.26 mg·m^{-3} down to 80 meters during July through September. Similar comparisons with vertical distributions presented in Radenac and Rodier (1996) exhibited the same general agreement for January 1986 (observed: surface bloom concentrations of 0.1-0.2 mg·m^{-3} with a subsurface maximum concentration > 0.5 mg·m^{-3}), July 1987 (observed: pronounced subsurface maximum concentrations > 0.4 mg·m^{-3}), March-April 1988 (observed: surface bloom concentrations > 0.2 mg·m^{-3}), and December 1989 (observed: surface bloom concentrations > 0.2 mg·m^{-3}). Overall, there are two general profiles observed, (1) low surface concentrations, i.e., chlorophyll-a < 0.1, with a pronounced DCM and (2) a surface bloom situation, i.e., chlorophyll-a > 0.1, with a reduced DCM.

Zooplankton distributions (Figure 7) are difficult to corroborate. The model indicates extreme variability with peak concentrations near the surface during surface bloom conditions. On average, zooplankton nitrogen in the surface layer was about 0.12 mg-atN·m^{-3} with no pronounced subsurface maximum. When the model is run with no vertical advection and minimal vertical diffusion, both phytoplankton and zooplankton exhibit uninterrupted subsurface

maxima near 100 m. Vinogradov et al. (1972) indicate that the ratio of total phytoplankton to herbivore biomass (cal·m^{-2}) in the upper 200 m is about 1.3. The model ratio based on the climatological profiles of P and Z nitrogen is 1.3 in the uppermost 90 m where 89% of the gross production occurs.

As shown in Figures 6a and 17, the model MLD is generally around 42 meters and maximum K$_v$ values coincide with that layer. Thus, with deep mixing rarely occurring, NO$_3^-$ is nearly depleted in the surface layer (Figures 7 and 9). The 5 mg-atN·m^{-3} isopleth was on average below 130 meters, but did shoal to the surface in 1988. Nonetheless, large amplitude displacements of the order of 150 m in the nitracline do occur on the decadal scale. The depth of the 5 mg-atN·m^{-3} isopleth is consistent with the 4 cases presented by Radenac and Rodier (1996) and the climatological profile is similar to that of Conkright et al. (1994), especially in the mixed layer and near 250 m. Barber and Chavez (1991) report 60 m NO$_3^-$ to be about 0.30 mg-atN·m^{-3}. The mean model value at 60 m was 0.91 mgN-at·m^{-3} (the Conkright et al. (1994) climatological value is 1.36 mg-atN·m^{-3}).

NH$_4^+$ (Figures 7 and 9) exhibits a subsurface maximum with concentrations as high as 0.5 mg-atN·m^{-3} at depth. Surface NH$_4^+$ concentrations peak concurrently with zooplankton concentrations during phytoplankton bloom conditions. Data from J. Murray (personal communication) collected in April 1996 show a subsurface maximum at 100 m with values > 0.3 mg-atN·m^{-3}. The average model NH$_4^+$ profile has a constant value near 0.11 mg-atN·m^{-3} in the surface layer and a subsurface maximum of 0.19 mg-atN·m^{-3} at 110 m.

As mentioned in the introduction, most primary productivity climatologies indicate the western Pacific to have very low production values of the order of 30-40 gC·m^{-2}·yr^{-1}. Barber and

Chavez (1991) estimate the production to be 90-120 gC·m⁻²·yr⁻¹. Figure 10 provides the time series of annual gross, net, and new production. Gross production ranged between 40 (1987 and 1992) and 250 (1984 and 1989) gC·m⁻²·yr⁻¹ and averaged 140 gC·m⁻²·yr⁻¹. New production ranged between 17 (1987 and 1992) and 48 (1988 and 1992) gC·m⁻²·yr⁻¹ with a mean of 31 gC·m⁻²·yr⁻¹ indicating an average f-ratio of 0.22. The average new production value at 165°E is about twice the 14.5-16 gC·m⁻²·yr⁻¹ value of Peña et al. (1994) for the entire tropical Pacific warm pool encompassed by the 26°C isotherm.

Primary production is proportional to the C:Chl-a ratio and growth rate. The climatological C:Chl-a profile decreased from 110 μgC/μgChl-a at the surface to a minimum of 34 μgC/μgChl-a at 160 m. The euphotic depth is defined as the depth at which E(PAR) is 1% of the surface value, E_o^-(PAR) for daylight hours. The average euphotic depth was 128 m and the mean euphotic zone C:Chl-a ratio was 53 μgC/μgChl-a. Chavez et al. (1991) report a value of 57 for 140°W. Barber and Chavez (1991) report a mean euphotic zone growth rate (24-hr. incubations under natural light) of 0.27 d⁻¹ which is essentially the same as that predicted by the model, 0.26 d⁻¹. Table 3 provides a summary of comparisons of model and observed quantities.

Ecosystem Processes and Interactions

Given the existence of the DCM and the low nutrient concentrations near the surface, the question is at what depth does growth limitation transition from nutrient limitation to light limitation, i.e., where does L_{lim} become less than N_{lim}. Nutrient limitation is defined as the maximum of NO_{3lim} and NH_{4lim}. Figure 11a shows the climatological profiles of both. On average, NH_{4lim} exceeds NO_{3lim} in the upper 120 m. However, as indicated in Figure 11b, light,

L_{lim}, becomes limiting, on average, at about 110 m which is just below the DCM. Convergence

of these two terms is rapid as each is trending strongly in opposite directions at this depth. Thus,

not surprisingly, nutrient limitation dominates over the depth range where most primary

production (95%) is occurring. Also, the broad gap between the two curves implies that highly

accurate values for the surface irradiance are not nearly as crucial at this location as would be

required at high latitudes where light limitation is more severe.

An analysis was performed on the ecosystem model to quantify the nitrogen fluxes in and

out of each of the ecosystem components (P, Z, NO_3^-, NH_4^+), and to verify that nitrogen is

conserved. The products of this analysis consist of (1) a composite time series of total stored

nitrogen in the system, vertical diffusive and advective fluxes, and the nitrogen flux due to all

biological sources and sinks combined (Figure 12); (2) a flow chart diagram of the

climatological, interactive nitrogen fluxes within the ecosystem and through the bottom boundary

(Figure 3); and, (3) climatological vertical profiles of the nitrogen concentration balance within

each of the four components of the ecosystem model (Figure 13).

The top panel of the time series in Figure 12 shows that the total nitrogen concentration in

the system has increased very slightly throughout the 9 years of simulation. The total increase

from the initial profile of nitrogen in the system (1330 mg-atN·m^{-2}), which is based on the

climatological NO_3^- profile and the initial conditions for the other components (Table 2) , is 191

mg-atN·m^{-2}, which is less than 1/3 standard deviation from the overall mean. This relatively

small increase is due the finite length of the time series with respect to the dominant scale of

interannual variability. The other two panels in Figure 12 show that most of the variance in the

system is due to the combined vertical advection and diffusion of nitrate (1.6 mg-atN·m^{-2}·d^{-1})

through the bottom boundary of the model. The combined sources and sinks have a significant climatological mean (1.5 mg-atN·m^{-2}·d^{-1}) but with a much lower temporal variability.

The flow chart in Figure 3 shows that there is a balanced exchange through the bottom boundary via the export of DON and PON from the system (-1.0 mg-atN·m^{-2}·d^{-1}), the sinking of fecal pellets (-0.6 mg-atN·m^{-2}·d^{-1}), and a net influx of nitrogen due to vertical diffusion and advection (1.6 mg-atN·m^{-2}·d^{-1}). Within the ecosystem itself, the balance is achieved by the multiple pathways of nitrogen fluxes in and out of the four model components. The largest fluxes are the phytoplankton nitrogen uptakes from the ammonium (11.8 mg-atN·m^{-2}·d^{-1}) and nitrate (4.3 mg-atN·m^{-2}·d^{-1}) pools. The advective fluxes of P and Z at the bottom boundary are zero by definition because of the Neumann boundary condition ($\partial X/\partial z = 0$) that is applied to these two components. This assumption does not impact the balances because both components approach very small values well above 250 m.

The vertical profiles in Figure 13 illustrate the relative importance of each term in the dynamic balance of each model component. Note that the scales for each component are not standardized. The values were derived by transposing all terms to the left side in equations 14-17 and computing the temporal averages at each depth. Some terms are relatively small and are not shown, e.g. advection and diffusion of P, Z, and NH$_4^+$. These four sets of profiles reveal that, as shown by the flowchart of Figure 3, the nitrogen uptake terms originating from the ammonium and nitrate pools are the largest contributors to the phytoplankton dynamic balance. In addition, the time-dependent terms are largest for the phytoplankton, ammonium, and nitrate components; the zooplankton component has much less temporal variability, except between 70 to 120 m, where most of the zooplankton variance occurs. While nitrification is relatively small, A^n attains

its maximum value at 90 m, on average. In summary, the first order terms in the dynamic

balances of each of the four components are: (a) phytoplankton - temporal change and nitrogen

uptake; (b) zooplankton - ingestion and respiration; (c) ammonium - temporal change and

phytoplankton uptake; and, (d) nitrate - temporal change, phytoplankton uptake, vertical

diffusion, and vertical advection.

Assuming that the vertical advective and diffusive fluxes of nutrients control biological

processes in the Warm Pool, their relative contributions can be examine using the model. For

instance, the chlorophyll field obtained from a simulation where w = 0 is shown in Figure 14.

This simulation produces a constant well-defined DCM at about 90 m. In this case, surface

chlorophyll exceeds 0.25 $mg \cdot m^{-3}$ only during the brief periods during the winters of 1988 and

1990 when intense surface mixing ($K_v > 100$ $m^2 \cdot d^{-1}$) penetrated deeper than 70 m. As for

upwelling, because vertical motions occur at all depths, the question is at what depth are the

vertical motions most influential. The climatological upwelling maxima is at 35 m (Figure 6b)

with weak downwelling below 75 m. A cross correlation analysis (Figure 15) of surface

chlorophyll and vertical NO_3^- advection (all depths) indicates that the surface chlorophyll

concentration is significantly influenced by the vertical velocity at all lags and depths above 70 m

and at depths below 70 m for negative lags (in advance of chlorophyll) earlier than -20 days. A

similar cross correlation analysis of surface chlorophyll versus vertical NO_3^- diffusion (Figure 16)

demonstrates that diffusion is effective only above 100 m. Surface blooms would be the result of

the transport of both nutrients and phytoplankton from the DCM to much shallower depths and

the two processes can work in concert (example, the bloom during 1988-1989), alone (example:

upwelling forced in 1984) or in opposition (example: absence of late 1986 surface bloom in

Figure 7 versus the pronounced 'diffusion only" bloom indicated in Figure 14).

Biological feedbacks and penetration radiation

In the present uncoupled implementation of the OGCM, the feedbacks from the biology

to physical fields, such as described in Siegel et al. (1995), cannot be addressed, especially if the

processes are on short time scales. However, assuming that on seasonal and interannual time

scales the OGCM temperatures near the surface approximate the actual temperatures, then the

effect of pigment concentration variability should be noticeable if local absorption has any

significant influence on temperature. However, there does not appear to be any correspondence

between SST and surface chlorophyll concentration even though model concentrations vary 30-

fold. This supports the same conclusion for the Warm Pool drawn by Leonard and McClain

(1996) using AVHRR temperature and CZCS pigment data products.

Recently, there has been much discussion about an apparent imbalance in the tropical

Pacific heat budget. Lewis et al. (1990) show that the radiation penetrating through the mixed

layer is sufficient to explain the imbalance while Ramanathan et al. (1995) invoke anomalous

cloud absorption effect. For the western Pacific, Lewis et al. estimated a penetration radiation of

20 $W \cdot m^{-2}$. Ohlman et al. (1996) extended the analysis of Lewis et al. to encompass the global

ocean and also show that in the tropics the penetration radiation can be of the order of 20 $W \cdot m^{-2}$.

Figure 17 provides the time series of daily average penetration irradiances indicating a

climatological mean of 18 $W \cdot m^{-2}$ or about 8% of the mean total irradiance.

Ecosystem and mixed layer models such as McClain et al. (1996) and Chen et al. (1994),

respectively require the diffuse attenuation coefficient, K(PAR) to calculate light attenuation and

the penetration irradiance. The temporal average model values of K(PAR) over the first 10 meters and over the mixed layer were 0.079 m^{-1} and 0.057 m^{-1}, respectively. Nonspectral ecosystem models commonly apply an empirical expression for K(PAR) by Morel (1988) which yields an average value of 0.044 m^{-1} when applied to the model surface chlorophyll time series (the surface value is essentially the same as the mean mixed layer value). The Morel relationship results in a slightly higher value of 0.048 m^{-1} for a concentration of 0.12 mg·m^{-3}, the temporal mean value in the mixed layer (Table 3). K(PAR) does tend to decrease with depth for a given chlorophyll concentration as water absorption selectively attenuates the longer wavelengths. This comparison points out the fact that care should be taken when employing approximate empirical relationships such that given in Morel (1988).

Conclusions

The primary purpose of this study was to examine the interannual biological variability in the Warm Pool using a simple ecosystem model with realistic forcing from an OCGM. The model reproduces, on average, the observed chlorophyll and nitrate profiles. There is inadequate in situ data to evaluate the zooplankton and ammonium results, although the model does generate a realistic ammonium profile having a distinct subsurface maximum that is not an artifact of the bottom boundary condition. Other quantities such as average C:Chl-a and phytoplankton growth rate are similar to the observed values.

The model indicates that interannual variability is dramatic with surface chlorophyll concentrations changing by a factor of 30. This variability appears to be controlled primarily by variations in the vertical advection of NO$_3^-$, especially below 100 m. However, on average,

vertical advection results in a net loss of nitrogen which is offset by deep diffusion upwards through the bottom boundary. The remainder of the balance is achieved through losses via the DON, PON, and fecal pellet pools which are not explicitly tracked in the model but are assumed to be transported out of the system through the bottom boundary. Annual primary productivity fluctuates by a factor of six on interannual time scales. On average the productivity is about 3-4 times the value found in climatological estimates, but is more in line with recent values of over 100 gC·m^{-2}·yr^{-1}. New production is about 20% of the gross production.

The mean penetration irradiance of about 18 W·m^{-2} is essentially the same as the value of about 17 W·m^{-2} estimated by Lewis et al. (1990). This agreement is extraordinary because the two methods used different estimates of surface irradiance, MLD, and diffuse attenuation coefficients. The penetration irradiance is about 8% of the total irradiance that enters the water column and cannot be ignored when considering the Warm Pool heat budget.

References

Baker, K. S. and R. C. Smith, Bio-optical classification and model of natural waters, 2, *Limnol. Oceanogr.*, 27, 500-509, 1982.

Barber, R. T. and F. P. Chavez, Regulation of primary productivity rate in the equatorial Pacific, *Limnol. Oceanogr.*, 36, 1803-1815, 1991.

Berger, W. H., Global maps of ocean productivity, *Productivity of the Ocean: Present and Past*, (W. H. Berger, V. S. Smetacek and G. Wefer, eds.), John Wiley & Sons, New York, 429-455, 1989.

Bishop, J. K. B. and W. B. Rossow, Spatial and temporal variability of global surface solar irradiance, *J. Geophys. Res.*, 96, 16,839-16,858, 1991.

Bishop, J. K. B., W. B. Rossow, and E. G. Dutton, Surface solar irradiance from the International Satellite Cloud Climatology Project 1983-1991, *J. Geophys. Res.*, 102, 6883-6910, 1997.

Blanchot, J., M. Rodier and A. Le Bouteiller, Effect of El Niño Southern Oscillation events on the distribution of phytoplankton in the western Pacific tropical ocean, *J. Plankton Res.*, 14, 137-156, 1992.

Chavez, F. P. and R. T. Barber, An estimate of new production in the equatorial Pacific, *Deep-Sea Res.*, 34, 1229-1243, 1987.

Chavez, F. P., K. R. Buck, K. H. Coale, J. H. Martin, G. R. DiTullio, N. A. Welschmeyer, A.C. Jacobson, and R. T. Barber, Growth rates, grazing, sinking, and iron limitation of equatorial Pacific phytoplankton, *Limnol. Oceanogr.*, 36, 1816-1831, 1991.

Chavez, F. P., K. R. Buck, S. K. Service, J. Newton, and R. T. Barber, Phytoplankton variability in the central and eastern tropical Pacific, *Deep-Sea Res., Part II*, 43, 835-870, 1996.

Chen, D., A. Busalacchi, and L. Rothstein, The roles of vertical mixing, solar radiation, and wind stress in a model simulation of the sea surface temperature seasonal cycle in the tropical Pacific Ocean, *J. Geophys. Res.*, 99, 20,345-20,359, 1994.

Cloern, J., C. Grenz, and L. Vidergar-Lucas, An empirical model of the phytoplankton chlorophyll:carbon ratio - the conversion factor between productivity and growth rate, *Limnol. Oceanogr.*, 40, 1313-1321, 1995.

Conkright, M., S. Levitus, and T. Boyer, NOAA Atlas NESDIS 1, World Ocean Atlas 1994, Vol. 1: Nutrients, U.S. Dept. of Commerce, 150 pp., 1994.

Cronin, M. and M. J. McPhaden, The upper ocean heat balance in the western equatorial Pacific

warm pool during September-December 1992, *J. Geophys. Res.*, 102, 8533-8553, 1997.

Dam, H. G., X. Zhang, M. Butler, and M. R. Roman, Mesozooplankton grazing and metabolism at the equator in the central Pacific: Implications for carbon and nitrogen fluxes, *Deep-Sea Res., Part II*, 42, 735-756, 1995.

Delcroix T. and C. Henin, Observations of the equatorial intermediate current in the western Pacific ocean (165E). *J. Phys Oceanogr.*, 18, 363-366, 1988.

Delcroix, T., and C. Henin, Seasonal and interannual variations of sea-surface salinity in the tropical Pacific ocean, *J. Geophys. Res.*, 96, 22,135-22,150, 1991.

Delcroix T., G. Eldin, M.H. Radenac, J. Toole and E. Firing, Variations of the western equatorial Pacific ocean, 1986-1988, *J. Geophys. Res.*, 97, 5423-5447, 1992.

Delcroix T., G. Eldin, M. McPhaden and A. Morliere, Effects of westerly wind bursts upon the western equatorial Pacific ocean, February-April 1991, *J. Geophys. Res.*, 98, 16379-16385, 1993.

Dobson, F. W. and S. D. Smith, Bulk models of solar radiation at sea, *Q. J. R. Meteorol. Soc.*, 114, 165-182, 1988.

Dupouy, C., J. Neveux, and J. M. André, Spectral absorption coefficient of photosynthetically

active pigments in the equatorial Pacific Ocean (165°E-150°W), *Deep-Sea Res., Part II*, 44, 1881-1906, 1997.

Eppley. R. W., Temperature and phytoplankton growth in the sea, *Fish. Bull.*, 70, 1063-1085, 1972.

Frouin, R., D. W. Lingner, C. Gautier, K. S. Baker and R. C. Smith, A simple analytical formula to compute clear sky total and photosynthetically available solar irradiance at the ocean surface, *J. Geophys. Res.*, 94, 9731-9742, 1989.

Furuya, K., Subsurface chlorophyll maximum in the tropical and subtropical western Pacific Ocean: vertical profiles of phytoplankton biomass and its relationship with chlorophyll *a* and particulate organic carbon, *Mar. Biol.*, 107, 529-539, 1990.

Garwood, R. W., An oceanic mixed-layer model capable of simulating cyclic states, *J. Phys. Oceanogr.*, 7, 455-471, 1977.

Gent, P., and M. A. Cane, A Reduced Gravity, Primitive Equation Model of the Upper Equatorial Ocean, *J. Comp. Phys.*, 81, 444-480, 1990.

Gent, P., 1991: The heat budget of the TOGA-COARE domain in an ocean model, *J. Geophys. Res.*, 96, Supplement, 3323-3330, 1991.

Gregg, W. W. and K. L. Carder, A simple spectral solar irradiance model for cloudless marine atmospheres, *Limn. Oceanogr.*, 35, 1657-1675, 1990.

Huang, R. X., Real freshwater flux as a natural boundary condition for salinity balance and thermohaline circulation forced by evaporation and precipitation, *J. Phys. Oceanogr.*, 23, 2428-2446, 1993.

Ikeda, T., Metabolic rates of epipelagic marine zooplankton as a function of body mass and temperature, *Mar. Biol.*, 85, 1-11, 1985.

Le Borgne, R., and M. Rodier, Net zooplankton and the biological pump: a comparison between the oligotrophic and the mesotrophic equatorial Pacific, *Deep-Sea Res., Part II*, 44, 2003-2023, 1997.

Leonard, C. L. and C. R. McClain, Assessment of interannual variation (1979-1986) in pigment concentrations in the tropical Pacific, *Int. J. Remote Sens.*, 17, 721-732, 1996.

Lewis, M. R., M.-E. Carr, G. C. Feldman, W. E. Esaias and C. R. McClain, Satellite estimates of the influence of penetrating solar radiation on the heat budget of the equatorial Pacific Ocean, *Nature*, 347, 543-545, 1990.

Lukas, R., and E. Lindstrom, The mixed layer of the western equatorial Pacific, *J. Geophys. Res.*, 96, 3343-3357, 1991.

Machey, D. J., J. Parslow, H. W. Higgins, F. B. Griffiths, and J. E. O'Sullivan, Plankton productivity and biomass in the western equatorial Pacific: Biological and physical controls, *Deep-Sea Res., Part II*, 42, 499-533, 1995.

Machey, D. J., J. S. Parslow, F. B. Griffiths, H. W. Higgins, and B. Tilbrook, Phytoplankton productivity and the carbon cycle in the western equatorial Pacific under El Niño and non-El Niño conditions, *Deep-Sea Res., Part II*, 44, 1951-1978, 1997.

McClain, C. R., A. R. Arrigo, K. S. Tai and D. Turk, Observations and simulations of physical and biological processes at OWS P, 1951-1980, *J. Geophys. Res.*, 101, 3697-3713, 1996.

McClain, C. R., S. R. Signorini, K-S. Tai, K. Arrigo, and R. Murtugudde, An ecosystem model for the simulation of physical and biological oceanic processes - IDAPAK user's guide and applications. NASA Tech. Memo. 206856, NASA Goddard Space Flight Center, Greenbelt, Maryland, 64 pp, 1998.

McPhaden M. and S. Hayes, On the variability of winds, sea surface temperature, and surface layer heat content in the western equatorial Pacific, *J. Geophys. Res.*, 96, 3331-3342, 1991.

Morel, A. Optical modeling of the upper ocean in relation to its biogenous matter content (case I waters), *J. Geophys. Res.*, 93, 10,749-10,768, 1988.

Murray, J. W., E. Johnson, and C. Garside, A U.S. JGOFS process study in the equatorial Pacific (EqPac): Introduction, *Deep-Sea Res., Part II*, 42, 275-293, 1995.

Murtugudde, R. G., Cane, M. A., and V. Prasad, A reduced gravity, primitive equation, isopycnal ocean GCM: formulation and simulations, *Mon. Wea. Rev.*, 123, 2864-2887, 1995.

Murtugudde, R., R. Seager and A. Busalacchi, Simulation of the tropical oceans with an ocean GCM coupled to an atmospheric mixed layer model, *J. Climate.*, 9, 1795-1815, 1996.

Murtugudde, R., and A. Busalacchi, Salinity effects in a tropical ocean model, *J. Geophys. Res.*, 103, 3283-3300, 1997.

Murtugudde, R., A. Busalacchi, and J. Beauchamp, Seasonal-to-interannual effects of the Indonesian throughflow on the tropical Indo-Pacific basin, *J. Geophys. Res.*, 103, 21,425-21,441, 1998.

Ohlmann, J. C., D. A. Siegel, and C. Gautier, Ocean mixed layer radiant heating and solar penetration: a global analysis, *J. Climate*, 9, 2265-2280, 1996.

Olson, R. J., Differential photoinhabition of marine nitrifying bacteria: a possible mechanism for the formation of the primary nitrite maximum, *J. Mar. Res.*, 39, 227-238, 1981.

Pacanowski, R. C., and G. H. Philander, Parameterization of vertical mixing in numerical models of tropical oceans, *J. Phys. Oceanogr.*, 11, 1443-1451, 1981.

Radenac, M.-H., and M. Rodier, Nitrate and chlorophyll distributions in relation to thermohaline and current structures in the western tropical Pacific during 1985-1989, *Deep-Sea Res., Part II*, 43, 725-752, 1996.

Palmer, T. N., and D. A. Mansfield, Response of two atmospheric general circulation models to sea-surface temperature anomalies in the tropical east and west Pacific, *Nature*, 310, 483-485, 1984.

Picaut, J., M. Ioualalen, C. Menkes, T. Delcroix, and M. J. McPhaden, Mechanism of the zonal displacements of the Pacific warm pool: implications for ENSO, *Science*, 274, 1486-1489, 1996.

Peña, M. A., M. R. Lewis, and J. J. Cullen, New production in the warm waters of the tropical Pacific Ocean, *J. Geophys. Res.*, 99, 14,255-14,268, 1994.

Ramanathan, V., B. Subasilar, G. J. Zhang, W. Conant, R. D. Cess, J. T. Kiehl, H. Grassl, and L. Shi, Warm Pool heat budget and shortwave cloud forcing: a missing physics?, *Science*, 267, 499-

503, 1995.

Seager, R., B. Blumenthal, and Y. Kushnir, An advective atmospheric mixed layer model for ocean modeling purposes: Global simulation of surface heat fluxes, *J. Climate.*, 8, 1951-1964, 1995.

Shiffer, R. A., and W. B. Rossow, ISCCP global radiance data set: a new resource for climate research, *Bull. Am. Meteorol. Soc.*, 66, 1498-1505, 1985.

Siegel, D. A., J. C. Ohlmann, L. Washburn, R. R. Bidigare, C. Nosse, E. Fields, and Y. Zhou, Solar radiation, phytoplankton pigments and radiant heating of the equatorial Pacific warm pool, *J. Geophys. Res.*, 100, 4885-4891, 1995.

Sprintall, J. and M. J. McPhaden, Surface layer variations observed in multiyear time series measurements from the western equatorial Pacific, *J. Geophys. Res.*, 99, 963-979. 1994.

Webster, P. J., and R. Lukas, TOGA-COARE: The Coupled Ocean-Atmosphere Response Experiment, *Bull. Am. Meteorol. Soc.*, 73, 1377-1416, 1992.

Xie, P., and P. Arkin, An intercomparison of guage observations and satellite estimates of monthly precipitation, *J. App. Meteorol.*, 34, 1143-1160, 1996.

Vinogradov, M. E., V. V. Menshutkin and E. A. Shushkina, On mathematical simulation of a pelagic ecosystem in tropical waters of the ocean, *Mar. Biol.*, 16, 261-268, 1972.

Zeebe, R. E., H. Eicken, D. H. Robinson, D. Wolf-Gladrow, and G. S. Dieckmann, Modeling the heating and melting of sea ice through light absorption by microalgae, *J. Geophys. Res.*, 101, 1163-1181, 1996.

Tables

TABLE 1

Environmental data required for the computation of the spectral surface irradiance.

Radiative Transfer Model Ancillary Data			
Parameter	Data Source	Sampling Frequency	Default Value
Surface Wind Speed	ECMWF	Monthly	
Relative Humidity	Bishop & Rossow (1991)		80%
Visibility	Bishop & Rossow (1991)		25 km
Precipitable Water	ISCCP		4.84 cm
Surface Pressure			1013 mb
Ozone	ISCCP		260 DU

TABLE 2

Ecological Model Variables and Input Parameter Definitions and Values. For OWS P, "original" and "spectral" refers to the values used in McClain et al. (1996) and McClain et al. (1998), respectively.

Symbol	OWS P (original)	OWS P (spectral)	Warm Pool (spectral)	Definition
				Derived Quantities
P				Phytoplankton nitrogen, mg-atN·m⁻³
Z				Zooplankton nitrogen, mg-atN·m⁻³
NO_3				Nitrate, mg-atN·m⁻³
NH_3				Ammonium, mg-atN·m⁻³
G				Phytoplankton growth rate, d⁻¹
π_1				Regenerated production fraction
π_2				New production fraction
I				Zooplankton grazing rate, d⁻¹
				Initial Conditions
			0.1	Initial P concentration, mg-atN·m⁻³
			0.1	Initial Z concentration, mg-atN·m⁻³
			Climatology	Initial nitrate concentration profile, mg-atN·m⁻³
			0.1	Initial ammonium concentration, mg-atN·m⁻³
				Phytoplankton Input Parameters
m	0	0.1	0.1	Death rate, d⁻¹
G_0	0.851	0.851	0.591	Growth rate at 0°C, d⁻¹
k_{gp}	0.0633	0.0633	0.0633	Temperature sensitivity of algal growth, 1/°C
η	0.02	0.02	0.02	Respiration coefficient, dimensionless
k_{rp}	0.0633	0.0633	0.0633	Temperature sensitivity of algal respiration, 1/°C
I_{kmax} (<60m)	25.0	25.0	400.0	Maximum photoacclimation parameter, µEin·m⁻²·s⁻¹
I_{kmax} (≥60m)	250.0	160.0	400.0	
K_{NO3}	1.0	1.0	1.0	Half saturation for nitrate uptake, mg-atN·m⁻³
K_{NH4}	0.1	0.1	0.5	Half saturation for ammonium up-take, mg-atN·m⁻³

pk	3.0	5.0	5.0	Ammonium inhibition of nitrate uptake, dimensionless
S_{max}	1.0	1.0	0	Maximum sinking rate, $m \cdot d^{-1}$
chla:N	1.0	1.0	1.0	Chlorophyll-a:Nitrogen ratio, $mg \cdot mg\text{-}atN^{-1}$

Zooplankton Input Parameters

g	0.04	0.075	0.04	Death rate, d^{-1}
R_m	5.0	4.75	7.0	Maximum grazing rate, d^{-1}
Λ	0.8	0.8	0.8	Ivlev constant, $m^3 \cdot mg\text{-}atN^{-1}$
TH	0.0	5.0	0.0	Minimum C threshold for grazing, $mgC \cdot m^{-3}$
γ	0.3	0.3	0.3	Unassimilated ingested ration, dimensionless
r_{zo}	0.019	0.019	(reformulated)	Respiration rate at $0^{\circ}C$, d^{-1}
k_{rz}	0.15	0.15	(reformulated)	Temperature sensitivity of respiration, $1/^{\circ}C$

Nutrient Input Parameters

a_z	0.5	0.6	0.6	Fraction of dead zooplankton converted to ammonium
a_p	0.5	0.6	0.6	Fraction of dead phytoplankton converted to ammonium
A^n_{max}		2.0	2.0	Maximum rate of nitrification, $nmol \cdot d^{-1}$
D_{min}		0.0095	0.0095	Minimum irradiance (300-470 nm) for nitrification, $W \cdot m^{-2}$
K_D		0.036	0.036	Half-saturation dosage for nitrification photoinhibition, $W \cdot m^{-2} \cdot nm^{-1}$
c_{pel}		0.8	0.8	Fecal pellet remineralization fraction

Physical Parameters

Kv_{bot}	17.3	17.3	8.65	Minimum (bottom) eddy diffusion coefficient, $m^2 \cdot d^{-1}$

TABLE 3

Model - in situ comparisons at $(0°, 165°E)$. The mean euphotic depth (1% light level)
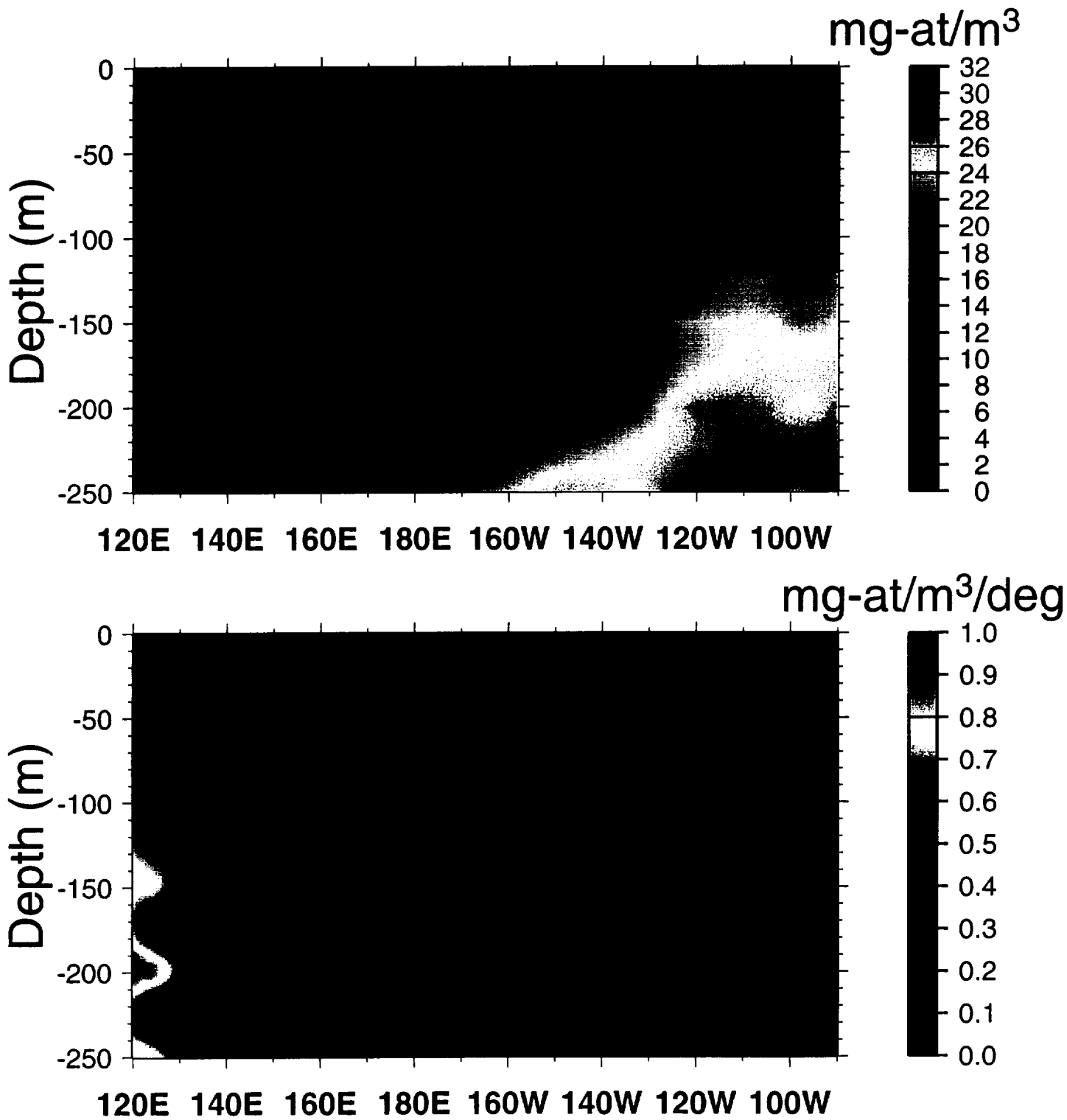
during daylight hours is 128 m.

PARAMETER	MODEL	OBSERVED
Mean Euphotic Zone C:Chl-a Ratio	53	57 (Chavez et al., 1991)
Primary Production $(gC \cdot m^{-2} \cdot yr^{-1})$	Gross: 140 (0-250 m)	90-120 (Barber & Chavez, 1991)
New Production $(gC \cdot m^{-2} \cdot yr^{-1})$	31 (0-250 m)	14.5-16: Warm Pool mean (Peña et al., 1994)
0-60 m Mean Chlorophyll Concentration $(mg \cdot m^{-3})$	0.12	0.10 (Barber & Chavez, 1991)
Depth of Deep Chlorophyll Maximum (m)	85 (Mean value)	75-125 (Barber & Chavez, 1991)
60 m NO_3^- Concentration $(mg\text{-}atN \cdot m^{-3})$	0.91	0.30 (Barber & Chavez, 1991) 1.36 (Conkright, et al., 1994)
Depth of NH_4^+ Maximum (m)	110	100 (Murray, unpublished)
Mean Euphotic Zone Growth Rate (d^{-1})	0.26	0.27 (Barber & Chavez, 1991)
Daily Mean Penetration Irradiance $(W \cdot m^{-2})$	18	17 (Lewis et al., 1990)

Figures

1. Equatorial transect of (a) nitrate (Conkright et al., 1994) and (b) the zonal derivative of nitrate, $\partial NO_3^-/\partial x$.

2. Time series of daily mean clear-sky irradiance $(E^c_F(PAR))$, ISCCP monthly mean cloud cover, and daily mean $E`_I(PAR)$. Daily mean values are 24 hour averages.

3. Ecosystem model flow diagram with climatological nitrogen fluxes $(mg\text{-}at\cdot m^{-2}d^{-1})$

4. Spectral absorption curves for water (Baker and Smith, 1982) and chlorophyll (Dupouy et al., 1997)

5. Depth-time contour plot of (a) $E`_I(PAR)$ in $\mu E\cdot m^{-2}\cdot s^{-1}$, (b) w $(m\cdot d^{-1})$, (c) K_v $(m^2\cdot d^{-2})$, and (d) temperature from the ocean general circulation model.

6. Climatological (a) K_v and (b) w profiles. Dashed lines indicate the ± 1 standard deviation boundaries, although K_v is never negative.

7. Depth-time contour plots of simulated (a) NO_3^-, (b) NH_4^+, (c) Z and (d) P (= chlorophyll-a) in $mg\text{-}atN\cdot m^{-3}$.

8. Annual mean profiles of chlorophyll-a.

9. Climatological profiles of (a) P (or chlorophyll-a), (b) Z, (c) NH_4^+, and (d) NO_3^- in $mg\text{-}atN\cdot m^{-3}$.

10. Time series of simulated annual gross, net, and new production.

11. Climatological model profiles of growth rate regulation factors, (a) NO_{3lim} and NH_{4lim}, and (b) L_{lim} and N_{lim}.

12. Depth-integrated nitrogen flux and total nitrogen time series, (a) total nitrogen $(P+Z+NO_3^-$ $+NH_4^+)$, (b) advective and diffusive fluxes with the rate of change in total nitrogen, and (c)
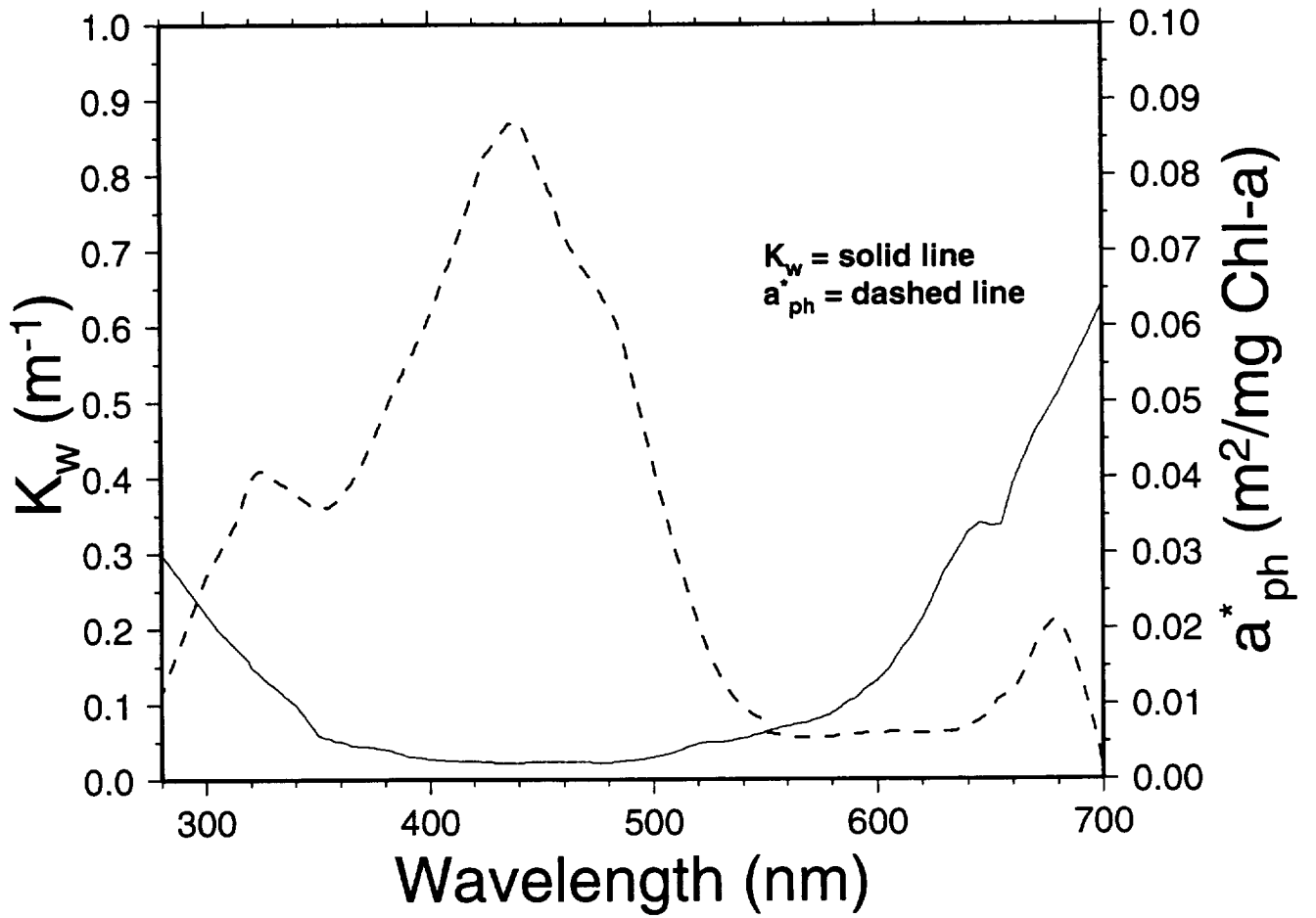
biological sources and sinks.

13. Climatological profiles of primary terms, i.e., terms making the largest contributions, in the ecosystem balance equations.

14. Depth-time contour plots for simulated (a) NO_3^-, (b) NH_4^+, (c) Z and (d) P (= chlorophyll-a) in mg·atN·m^{-3} derived from the w = 0 simulation.

15. Cross-correlation of vertical advective NO_3^- flux and surface chlorophyll concentration. Negative lags imply that advective flux leads chlorophyll concentration.

16. Cross-correlation of vertical diffusive NO_3^- flux and surface chlorophyll concentration. Negative lags imply that diffusive flux leads chlorophyll concentration.

17. Time series of mixed layer depth, subsurface $E^{\backprime}_I(PAR)$, i.e., just beneath the surface, and the ratio of the irradiance at the mixed layer depth to $E^{\backprime}_I(PAR)$. Because $E^{\backprime}_I(PAR) \approx E^{\backprime}_I(tot)/2$, the penetration irradiance has values of half the ratio shown.
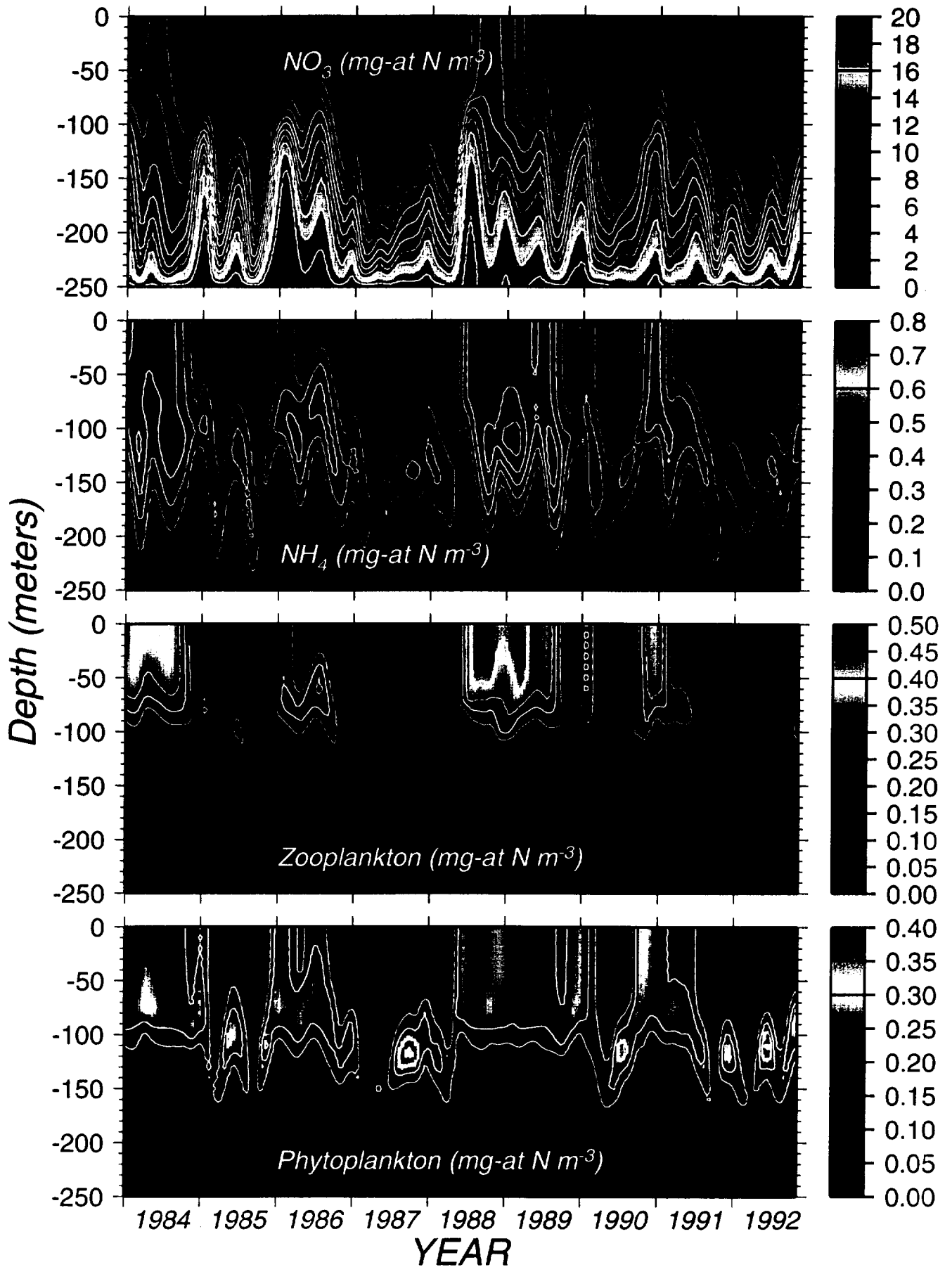
mg-at/m³

mg-at/m³/deg

GMT Oct 1 08:39   Nitrate and Absolute Nitrate Gradient (2.5°S-2.5°N average)

Fig. 5

CLIMATOLOGICAL ECOSYSTEM NITROGEN FLUX BALANCE
(mg-at N/m²/d)

Fig. 3

K_w = solid line
a^*_{ph} = dashed line

E_{PAR} (μEinsteins m^{-2} s^{-1})

w (m/day)

Vertical Diffusivity (m^2/day)

Temperature (^oC)

Depth (meters)

YEAR

GMT   Oct 1 14:33   30-Level OGCM, revised k_w, a^*_{ph}

Vertical Diffusivity (K_v in m^2 d^{-1})

Depth (meters)
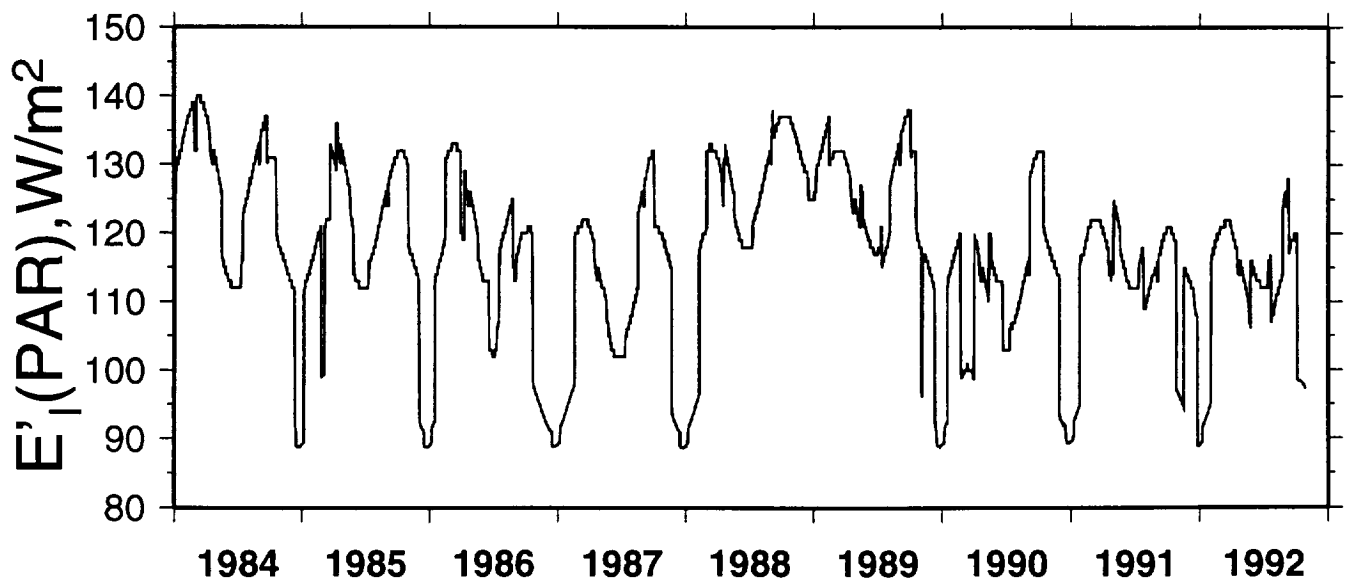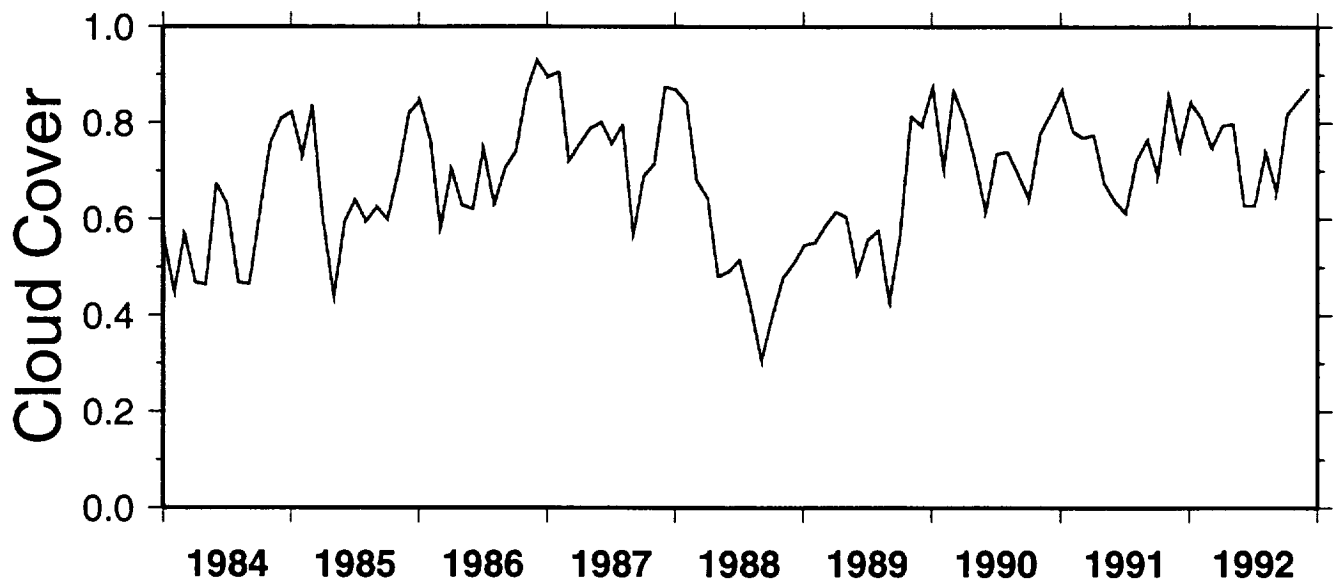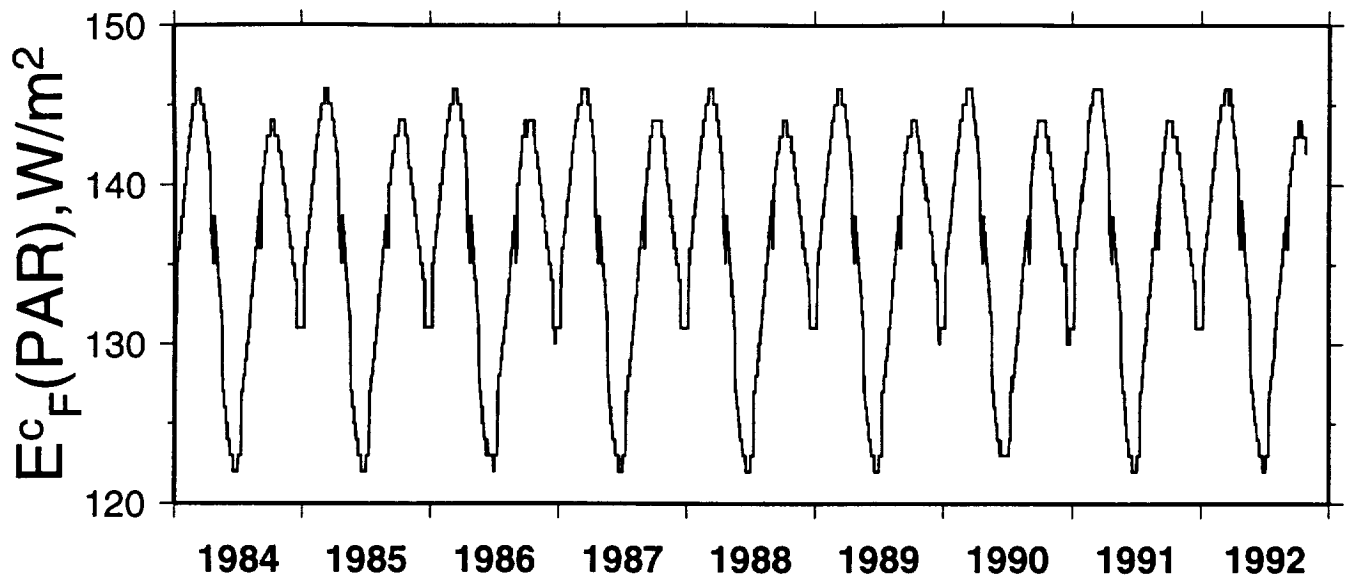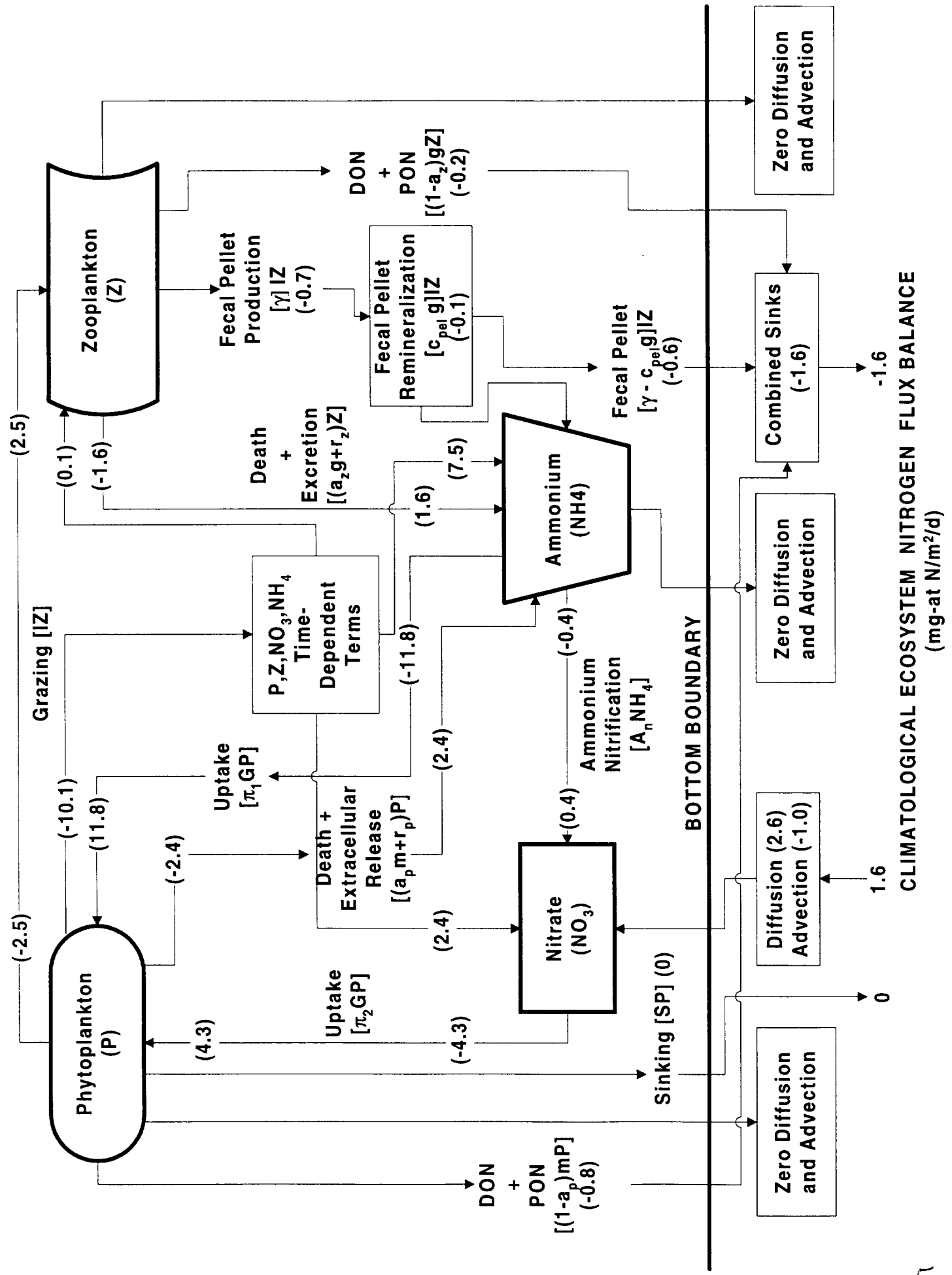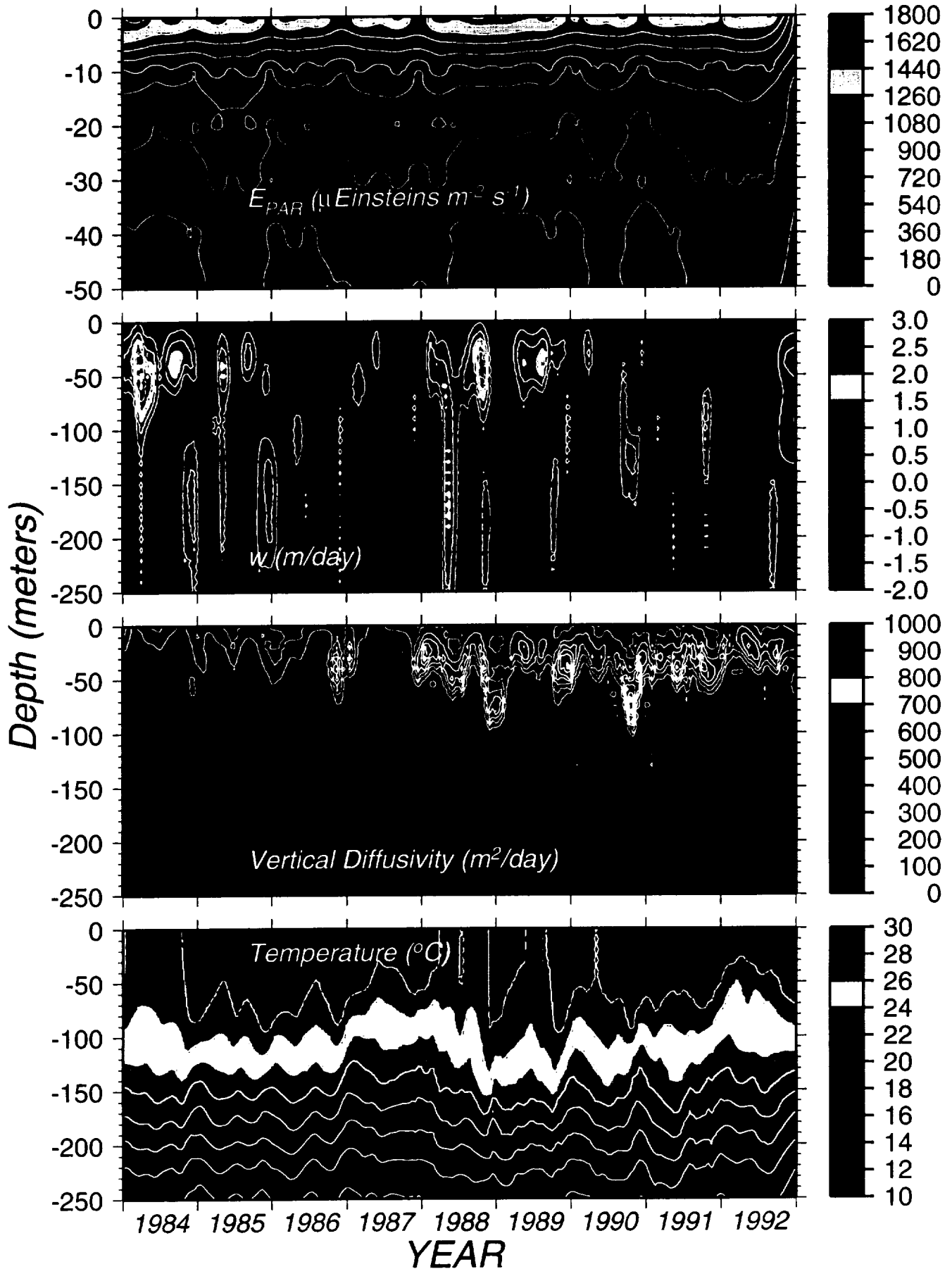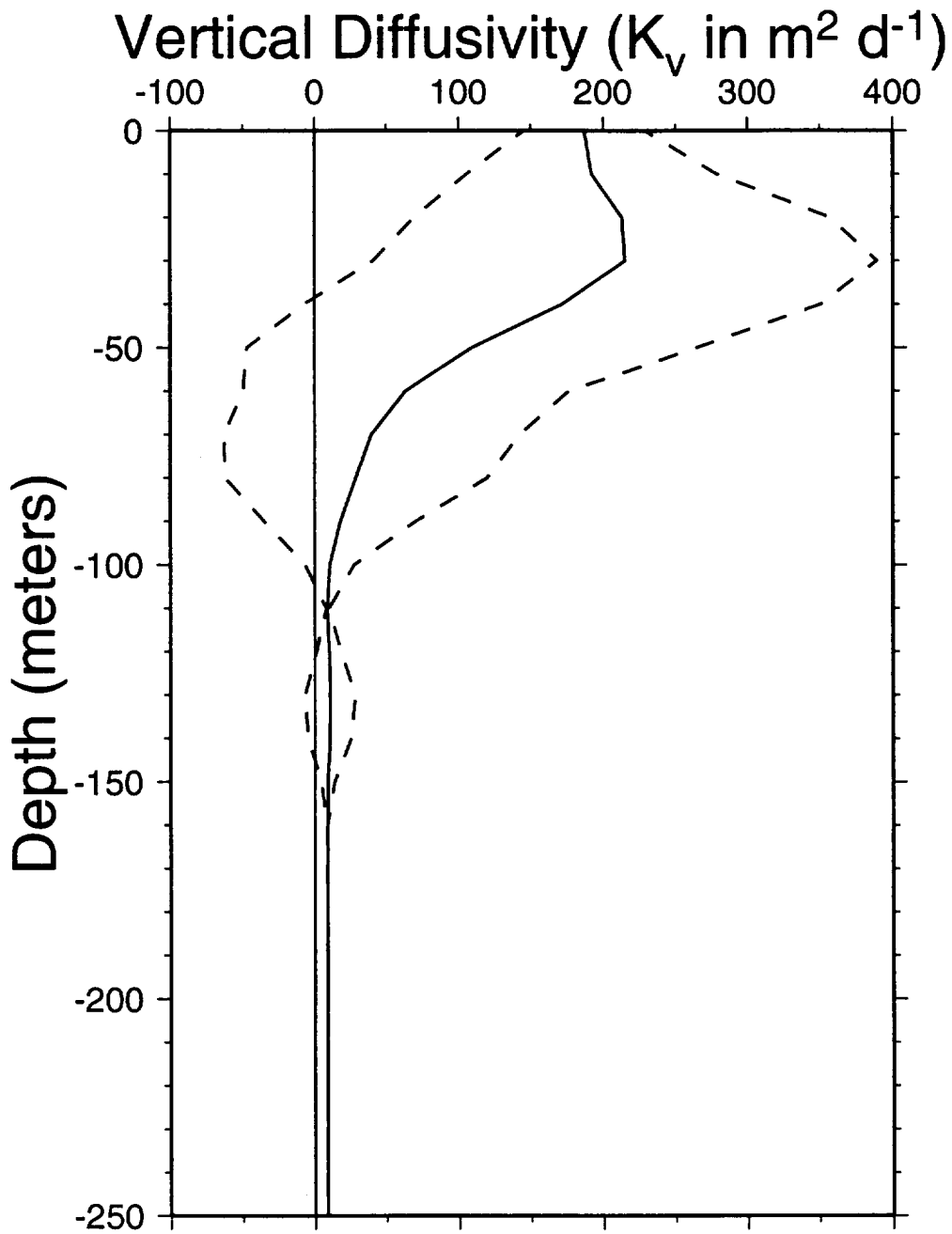
GMT Oct 6 11:26   Climatological Mean (84-92) of Kv(z) with monthly smoothing of OGCM products

Fig. 10

Vertical Velocity (w in m/d)
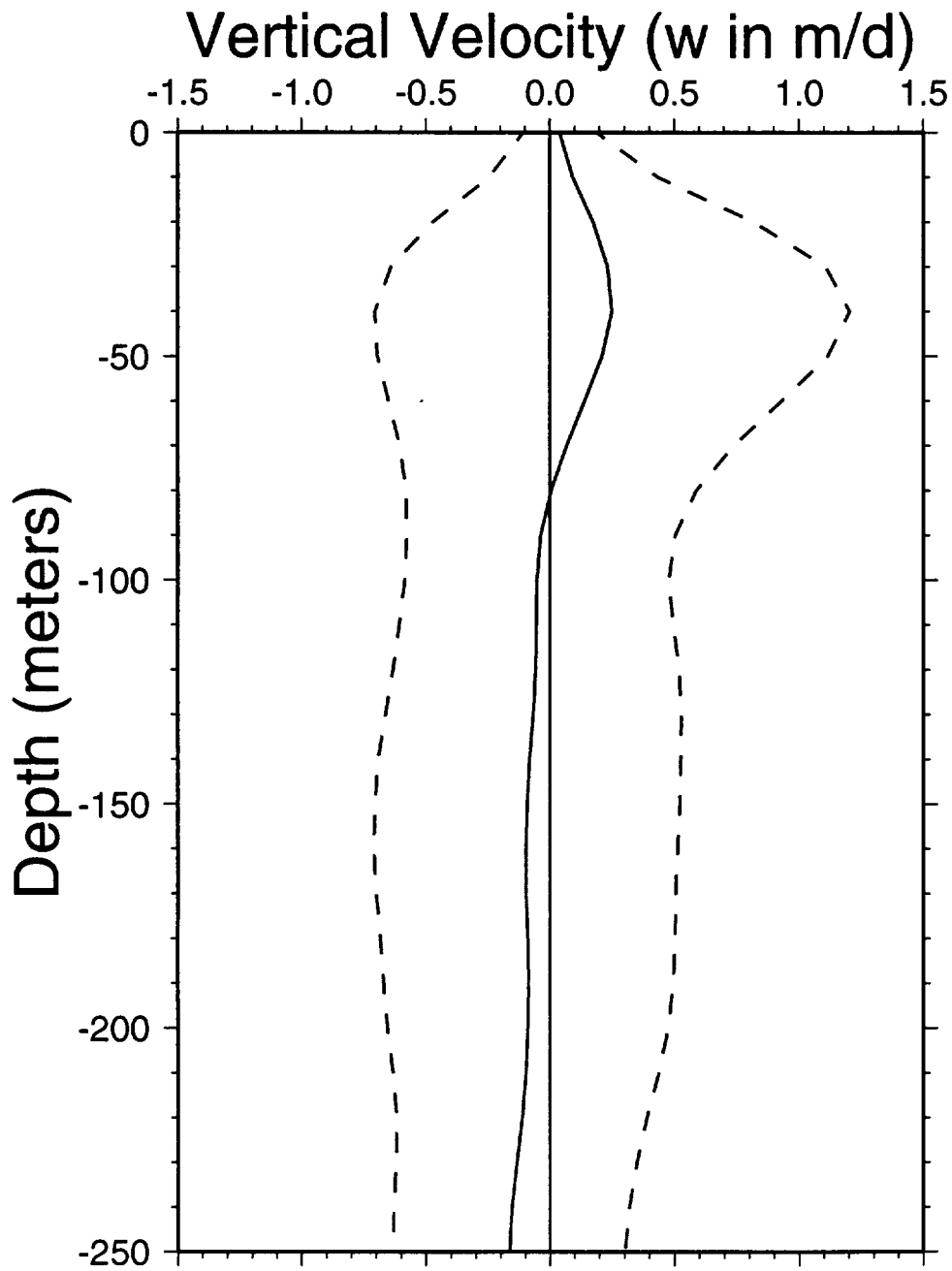
GMT Oct 6 11:23   Climatological Mean (84-92) of w(z) with monthly smoothing of OGCM products

Fig. 4b

NO$_3$ (mg-at N m^{-3})

NH$_4$ (mg-at N m^{-3})

Zooplankton (mg-at N m^{-3})

Phytoplankton (mg-at N m^{-3})

Depth (meters)

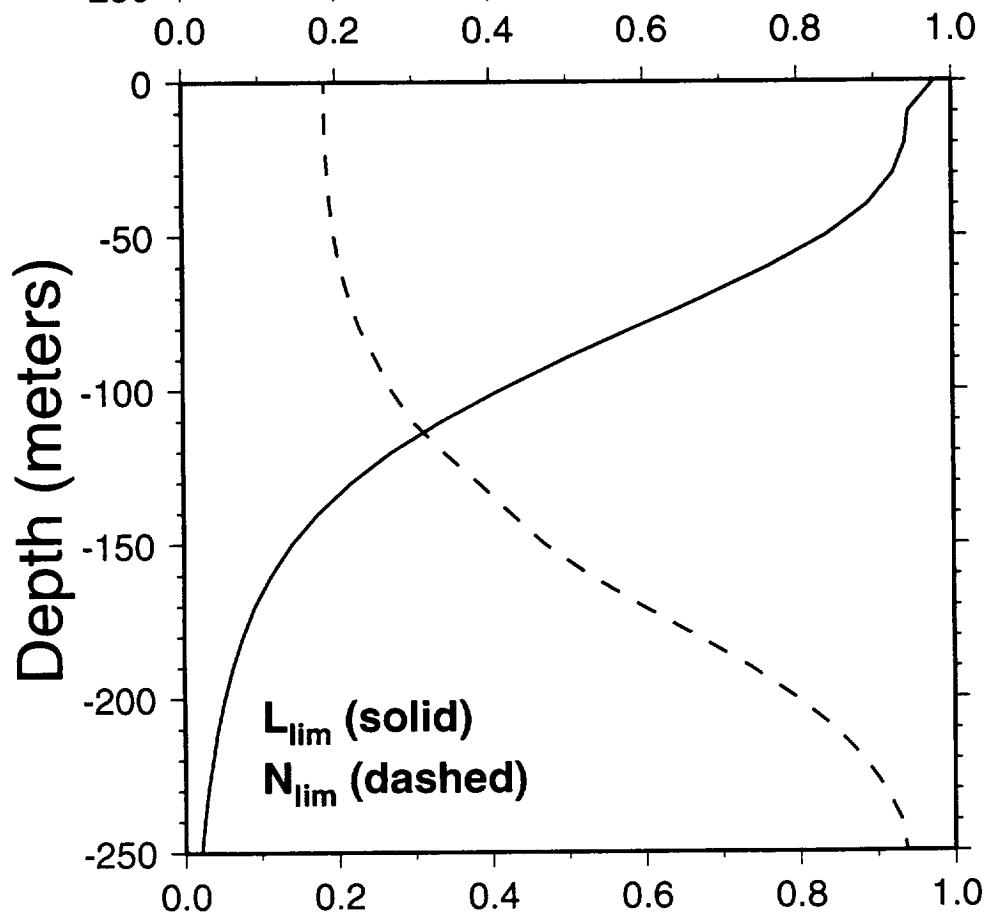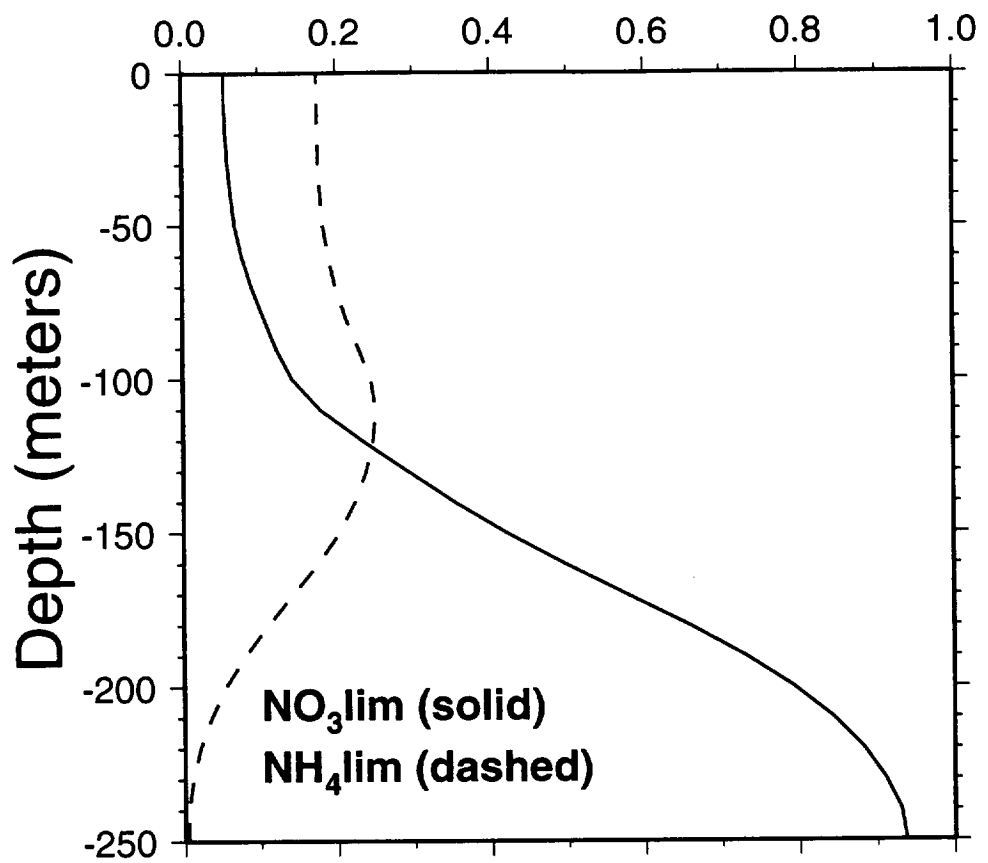YEAR

1984 1985 1986 1987 1988 1989 1990 1991 1992

GMT Sep 1 07:45   30-Layer OGCM, revised k$_w$, a$_{ph}$

Annual Mean Chl-a (mg-at N m^{-3})

Depth (meters)

1986

1988

PHYTO

ZOO

NH$_4$

NO$_3$ (Model)
(solid)
NO$_3$ (Conkright et al.)
(dashed)

GMT Oct 6 12:05   Climatological Mean (84-92) of P,Z,NH4,NO3 (mg-at N m^{-3}) using revised k$_w$, a$^*_{ph}$

Fig. 9

Gross Prod (solid)
(mean=140)
Net Prod (dashed)
(mean=116)
New Prod (dotted)
(mean=31)

Fig. 10

NO₃lim (solid)
NH₄lim (dashed)

L_lim (solid)
N_lim (dashed)

GMT Oct 6 11:40   Climatological Mean (84-92) of Llim, Nlim, NO3lim, and NH4lim with revised k_w, a^*_{ph}

Fig. 11

Mean N=1521 +/- 695 mg-at m^{-2} (solid)
Initial N=1330 mg-at m^{-2} (dashed)

wN = -1.0 mg-at/m^2/d (solid)
K∂N/∂z = 2.6 mg-at/m^2/d (dashed)

Σ(Sources+Sinks)Δz = -1.5 mg-at/m^2/d (dashed)
Σ(∂N/∂t)Δz = -0.07 mg-at/m^2/d (solid)

Fig 12

PHYTO

- ∂P/∂t
- GP
- mP
- r_pP
- IZ

ZOO

- ∂Z/∂t
- (1 − γ)IZ
- gZ
- r_zZ

NH$_4$

- ∂NH$_4$/∂t
- a_pmP
- r_pP
- π_1GP
- a_zgZ
- r_zZ
- c_{pel}γIZ

NO$_3$

- ∂NO$_3$/∂t
- w∂NO$_3$/∂z
- K∂²NO$_3$/∂z²
- π_2GP

Depth (meters)

GMT Oct 1 15:00 Climatological Mean (1984-1982) of equation terms (μg-at N m⁻³ d⁻¹) with revised k$_w$, a'$_{ph}$

Fig. 13

NO₃ (mg-at N m⁻³)

NH₄ (mg-at N m⁻³)

Zooplankton (mg-at N m⁻³)

Phytoplankton (mg-at N m⁻³)

Depth (meters)

YEAR

GMT Sep 1 13:38   30-Layer OGCM, revised k_w, a_ph and w=0

Cross-Correlation of Surface Chl-a vs. $w\partial NO_3/\partial z$(15, 245 m)

GMT Oct 6 12:26   30-level OGCM with k_w, a^*_{ph}

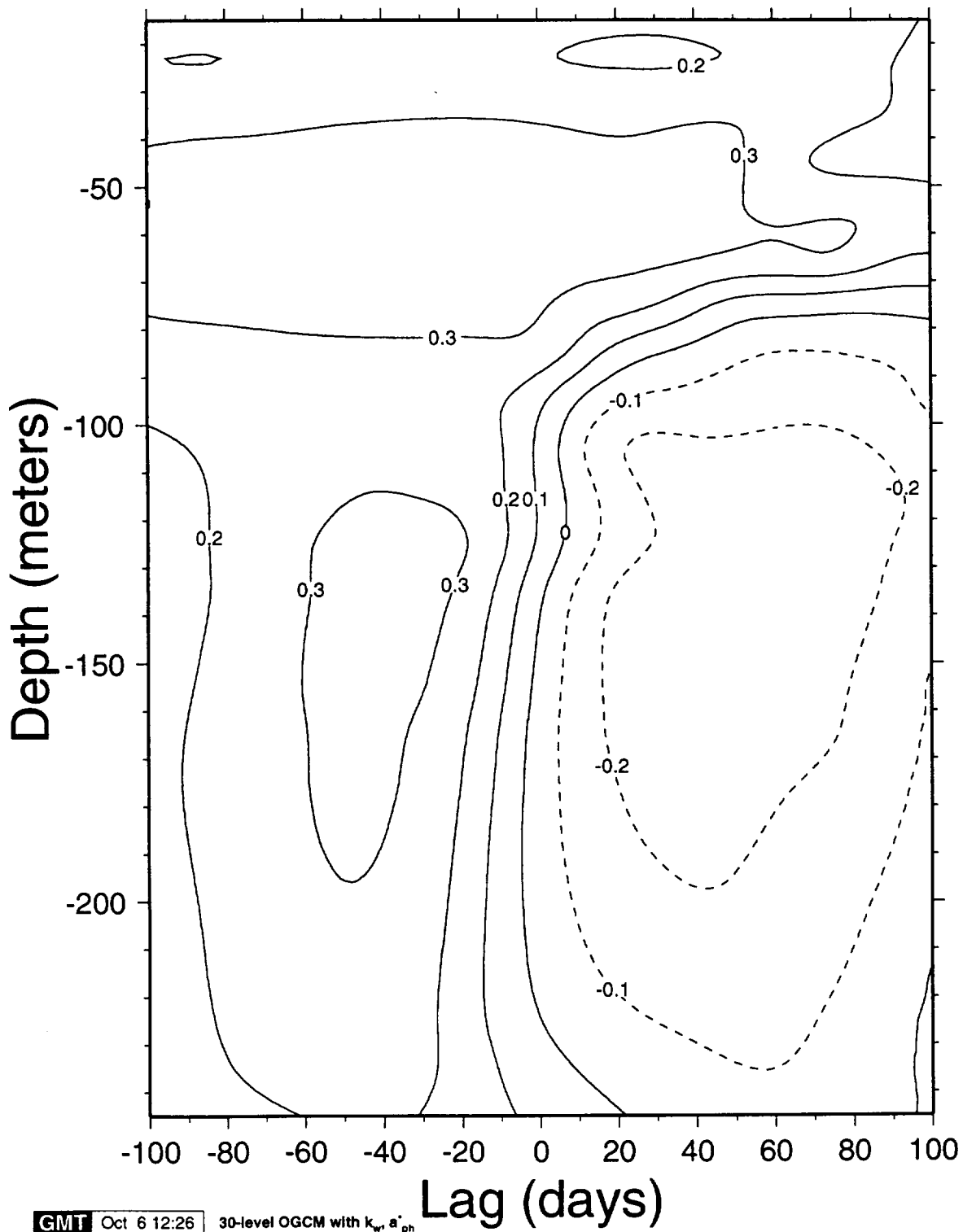Fig. 15

Cross-Correlation of Surface Chl-a vs. $K_v \partial^2 NO_3/\partial z^2$(15, 245 m)

Fig. 16

MLD (meters) — Mean MLD = 42.3 m

PAR (Watts m^{-2}) — $E_{PAR}(O^-)$ (mean=108.9), $E_{PAR}(mld)$ (mean=18.0)

$E_{PAR}(mld)/E_{PAR}(O^-)$ — Mean E_{MLD}/E_{PAR} = 0.17

YEAR

GMT Oct 6 12:20 Time series of light penetration variables with revised k_w, a'_{ph}

Fig. 17